

Imaging of angiogenesis  
with  $^{68}\text{Ga}$ -DOTA-RGD<sub>2</sub> PET/CT in  
squamous cell carcinoma of the  
head and neck

D. Lobeek

Master's Thesis Technical Medicine  
*Medical Imaging & Interventions*

20 May 2016

**Master thesis**

*Imaging of angiogenesis with  $^{68}\text{Ga}$ -DOTA-RGD<sub>2</sub> PET/CT in squamous cell carcinoma of the head and neck, May 2016*

Daphne Lobeek

**Graduation Committee**

Prof. dr. ir. C.H. Slump<sup>1</sup> (Chairman, Technical Supervisor)

Prof. dr. W.J.G. Oyen<sup>2,3</sup> (Medical and Technical Supervisor)

Prof. dr. O.C. Boerman<sup>2</sup> (Technical and Daily Supervisor)

Drs. P.A. van Katwijk<sup>4</sup> (Mentor)

Dr. ir. B. ten Haken<sup>5</sup> (External Supervisor)

**Institution**

<sup>1</sup> Department of Robotics and Mechatronics, University of Twente, Enschede, The Netherlands

<sup>2</sup> Department of Radiology and Nuclear Medicine, Radboud University Medical Center, Nijmegen, The Netherlands

<sup>3</sup> Institute of Cancer Research, Royal Marsden NHS Trust, London, United Kingdom

<sup>4</sup> Faculty of Science and Technology, University of Twente, Enschede, The Netherlands

<sup>5</sup> Department of NeuroImaging, University of Twente, Enschede, The Netherlands

---

This is a confidential document and is the property of Radboudumc. It contains unpublished data. No parts of this publication may be reproduced, stored in a retrieval system or transmitted in any form and by any means, without prior permission of the Radboudumc.

---

## Content

Summary	I
List of abbreviations	III
General introduction and outline of this thesis	1
Clinical background	1
Head and neck cancer	1
Treatment of head and neck cancer	2
Molecular pathways involved in (head and neck) cancer	3
Hallmarks of cancer	3
Angiogenesis	3
Process of angiogenesis	4
$\alpha_v\beta_3$ integrin expression	4
Imaging of $\alpha_v\beta_3$ integrin expression	6
Research questions	6
Outline of this thesis	7
Comparing DOTA-, TRAP-, fusarine-C-, and THP-conjugated $^{68}\text{Ga}$ -labeled RGD peptides	7
Introduction	7
Materials and method	11
Results	16
Discussion	20
Conclusion	21
$^{68}\text{Ga}$ -DOTA-RGD <sub>2</sub> PET/CT in HNSCC	23
Introduction	23
Study design	24
Materials and method	26
Preliminary results	27
Discussion	31
Conclusion	34
Appendix A: Approval of the Medical Ethical Committee for the 'RGD PET' study, correspondence number: NL52649.091.15 (2015-1813)	35
Appendix B: Supplementary data	43
General conclusion and future perspectives	45
Bibliography	49
Acknowledgements	55

## Summary

### Rationale

Head and neck cancer is the 7th and 9th most common cancer in men and in women, respectively, accounting for approximately 3,000 new cases in The Netherlands each year. Multimodality treatments involving surgery, radiotherapy, chemotherapy and molecular targeted therapies have expanded the therapeutic options for patients with head and neck cancer. Despite the advances in treatment possibilities, the five-years survival is poor and patients often show recurrence shortly after therapy. Angiogenesis is considered to play an important role in tumor growth and metastasis in these kind of tumors. With recent progress in Positron Emission Tomography Computed Tomography (PET/CT) imaging, it is possible to non-invasively image  $\alpha_v\beta_3$  integrin expression, an integrin on endothelial cells that is overexpressed during the process of angiogenesis. Tracers targeting angiogenesis might be of great value for treatment selection, guidance, and adaptation, aiming to individualize therapeutic options and prevent unnecessary side effects due to ineffective treatments. This study investigates the feasibility and safety of  $^{68}\text{Ga}$ -DOTA-RGD<sub>2</sub> PET/CT to image angiogenesis in patients with head and neck cancer.

### Objectives

The first objective of this thesis is to determine whether  $^{68}\text{Ga}$ -DOTA-RGD<sub>2</sub> is a viable radiotracer to image  $\alpha_v\beta_3$  integrin expression. The second objective of this thesis is to propose a study design to ascertain the feasibility and safety to image tumor angiogenesis in head- and neck cancer patients using  $^{68}\text{Ga}$ -DOTA-RGD<sub>2</sub> PET/CT.

### Methods

The  $\alpha_v\beta_3$  integrin targeting characteristics of  $^{68}\text{Ga}$ -DOTA-RGD<sub>2</sub> are compared with three other promising radiotracers ( $^{68}\text{Ga}$ -TRAP-RGD<sub>3</sub>,  $^{68}\text{Ga}$ -FSC-RGD<sub>3</sub>, and  $^{68}\text{Ga}$ -THP-RGD<sub>3</sub>). All four radiotracers are labeled with Gallium-68, and the binding affinity of the four radiotracers is determined *in vitro*, using a solid phase competitive binding assay. Subsequently, the *in vivo*  $\alpha_v\beta_3$  integrin targeting characteristics of the four radiotracers are determined, using mice with subcutaneously growing  $\alpha_v\beta_3$  integrin-expressing tumors.

A prospective, observational, non-randomized feasibility study is proposed to study the feasibility and safety of  $^{68}\text{Ga}$ -DOTA-RGD<sub>2</sub> PET/CT. 25 patients undergo a  $^{68}\text{Ga}$ -DOTA-RGD<sub>2</sub> (200 MBq, 70  $\mu\text{g}$ ) PET/CT scan before their planned surgical treatment. Three static PET/CT scans are acquired at 30, 60 and 90 minutes post injection in the first five patients. The following five patients undergo a dynamic PET/CT scan during 60 minutes. In the remaining 15 patients a static  $^{68}\text{Ga}$ -DOTA-RGD<sub>2</sub> PET/CT scan is acquired starting at the optimal scan time as determined in the first ten patients. Of all patients, histological samples are obtained to validate  $^{68}\text{Ga}$ -DOTA-RGD<sub>2</sub> as an imaging biomarker of angiogenesis.

### Results

All four radiotracers are produced with specific activities ranging from 40-48 MBq/nmol and a radiochemical yield of >95%. IC<sub>50</sub>-values were  $3.79 \pm 0.65$  nM,  $10.0 \pm 1.81$  nM,  $9.02 \pm 1.61$  nM, and  $11.38 \pm 1.88$  nM, for  $^{68}\text{Ga}$ -DOTA-RGD<sub>2</sub>,  $^{68}\text{Ga}$ -TRAP-RGD<sub>3</sub>,  $^{68}\text{Ga}$ -FSC-RGD<sub>3</sub>, and  $^{68}\text{Ga}$ -THP-RGD<sub>3</sub> respectively. Tracer accumulation in the tumors were respectively  $5.1 \pm 2.7$  %ID/g,  $4.3 \pm 0.8$  %ID/g,  $8.5 \pm 1.4$  %ID/g, and  $5.3 \pm 0.6$  %ID/g. Mice with  $^{68}\text{Ga}$ -FSC-RGD<sub>3</sub> showed a significantly higher concentration of the tracer

in blood. Consequently, tumor-to-blood ratios of  $^{68}\text{Ga}$ -DOTA-RGD<sub>2</sub> ( $17.81 \pm 9.39$ ),  $^{68}\text{Ga}$ -TRAP-RGD<sub>3</sub> ( $31.46 \pm 15.79$ ), and  $^{68}\text{Ga}$ -THP-RGD<sub>3</sub> ( $13.47 \pm 1.54$ ) were higher than those of  $^{68}\text{Ga}$ -FSC-RGD<sub>3</sub> ( $4.24 \pm 1.83$ ).

Until now,  $^{68}\text{Ga}$ -DOTA-RGD<sub>2</sub> was safely injected in two patients, showing no drug-related adverse events or changes in blood pressure, heart rate, and body temperature. Blood sampling indicated rapid blood clearance of the radiotracer, showing that the tracer is diffused from the blood to surrounding within 5 minutes. Maximum standardized uptake values ( $\text{SUV}_{\text{max}}$ ), as determined in tumor tissue of one patient, were of 5.9, 6.2, and 6.1, 30, 60, and 90 minutes post injection. Tumor-to-blood and tumor-to-muscle ratios at 60 minutes after injection were  $6.8 \pm 1.1$  and  $5.6 \pm 2.0$  respectively.

### Conclusion and discussion

$^{68}\text{Ga}$ -DOTA-RGD<sub>2</sub> and  $^{68}\text{Ga}$ -TRAP-RGD<sub>3</sub> showed optimal *in vitro* and *in vivo*  $\alpha_v\beta_3$  integrin targeting properties: good tumor-to-blood and tumor-to-muscle ratios, and lower tracer uptake in non-tumor tissue, compared to  $^{68}\text{Ga}$ -FSC-RGD<sub>3</sub> and  $^{68}\text{Ga}$ -THP-RGD<sub>3</sub>.  $^{68}\text{Ga}$ -DOTA-RGD<sub>2</sub> and  $^{68}\text{Ga}$ -TRAP-RGD<sub>3</sub> are therefore promising multimeric radiotracers for imaging of  $\alpha_v\beta_3$  integrin expression using PET/CT.

The preliminary findings in the first patients showed the potential of  $^{68}\text{Ga}$ -DOTA-RGD<sub>2</sub> PET/CT in HNSCC, as the tumor clearly showed enhanced tracer uptake compared to surrounding tissues. Furthermore, no adverse events related to the study drug were seen, indicating a safe procedure. Imaging of more patients is needed to provide further information on the validity of the results and conclusions drawn in this thesis. The results so far can be seen as a firm step towards a new non-invasive PET/CT imaging technique, that might be used to optimize treatment of head and neck cancer patients in future.

### List of abbreviations

%ID/g	Percentage injected dose per gram
$\alpha_v\beta_3$ integrin	Alpha-v-beta-three integrin
ALAT	Alanine aminotransferase
AIF	Arterial Input Function
APTAC	Arterial Plasma Time-Activity Curve
ASAT	Aspartaan aminotransferase
CAIX	Carbonic Anhydrase IX
CPM	Counts Per Minute
CT	Computed Tomography
DNA	Deoxyribonucleic acid
DOTA	1,4,7,10-tetraazadodecane-N,N',N'',N'''-tetraacetic acid
DOTAGA	DOTA derivative analogue of 1,4,7,10-tetraazadodecane-N,N',N'',N'''-tetraacetic acid
ECM	Extracellular Matrix
EGFR	Epidermal Growth Factor Receptor
F-18/ <sup>18</sup> F	Fluoride-18
<sup>18</sup> F-FDG	2-deoxy-2-( <sup>18</sup> F)fluoro-D-glucose
FFPE	Formalin-fixed and Paraffin-embedded Tissue Specimens
FOV	Field of View
Ga-68/ <sup>68</sup> Ga	Gallium-68
FSC	Fusarinine-C
GBM	Glioblastoma Multiforme
GCP	Good Clinical Practice
GLP	Good Laboratory Practice
GMP	Good Medicine Product
HIF1- $\alpha$	Hypoxia Inducible Factor Alpha
HNSCC	Head and Neck Squamous Cell Carcinoma
HPV	Human Papillomavirus
IC <sub>50</sub> -value	Half-maximal Inhibitory Concentration value
IDIF	Image-Derived Input Function
ITLC	Instant Thin-Layer Chromatography
<sup>111</sup> In/In-111	Indium-111
MMP	Matrix Metalloproteases
MRI	Magnetic Resonance Imaging
NOTA	1,4,7-triazacyclononane-triacetic acid
NODAGA	NOTA-derivatized chelating system
OSEM3D	Ordered Subset Expectation Maximisation 3-dimensional
p.i.	Post injection of $^{68}\text{Ga}$ -DOTA-RGD <sub>2</sub>
PET	Positron-Emission-Tomography
PORT	Post-Operative Radiotherapy
RGD	Arginine-glycine-aspartic acid
ROI	Region of Interest
RP-HPLC	Reversed-Phase High-Performance Liquid Chromatography
SPECT	Single Photon Emission Computed Tomography
Std/stdev	Standard Deviation
SUV	Standardized Uptake Value
SUV <sub>50%</sub>	Isocontouring of SUV of tumor volume, isocontour is set to 50%
SUV <sub>80%</sub>	Isocontouring of SUV of tumor volume, isocontour is set to 80%
SUV <sub>mean</sub>	Mean Standardized Uptake Value
SUV <sub>max</sub>	Maximal Standardized Uptake Value
SUV <sub>peak</sub>	A fixed threshold based method representing the eight voxels surrounding the SUV <sub>max</sub>
TGF- $\alpha$	Transforming Growth Factor-Alpha
TH	Thyroid Hormone
THP	1,6-dimethyl-3-hydroxypyridin-4-one groups
TRAP	1,4,7-triazacyclononane-1,4,7-tris[(2-carboxyethyl)-methylenephosphinic acid]
TTAC	Tissue-Time-Activity Curve
ULN	Upper limit of Normal
VEGF	Vascular Endothelial Growth Factor
VOI	Volume Of Interest

## Chapter 1: General introduction and outline of this thesis

### Clinical background

#### Head and neck cancer

Head and neck cancer is the 7th and 9th most common cancer in men and in women, respectively, accounting for approximately 3,000 new cases in The Netherlands each year [1]. Cancers of the head and neck region are divided into several types and subtypes based on the primary site of the tumor (Figure 1 and Table 1). It encompasses a diverse group of tumors that are frequently aggressive in their biologic behavior. Approximately 95% of all diagnosed head and neck cancer cases are histologically referred to as squamous cell carcinomas of the head and neck (HNSCC) [2]. Major risk factors for these kind of tumors are tobacco smoking, excessive alcohol consumption, and human papillomavirus (HPV) [3]. The choice of treatment of HNSCC depends on tumor size and site, stage of the disease, and expected oncological and functional outcomes (Table 1). Whereas early- and locally advanced tumors are often treated with surgery or radiotherapy, treatment of advanced HNSCC tumors often includes combinations of surgery, radiotherapy and chemotherapy. The quality of life of head and neck cancer patients is an important factor to consider in treatment choices of these patients. Quality of life is also influenced by side effects. Side effects of patients treated with surgery include swallowing and speech impairment, and loss of shoulder function. Patients treated with (chemo)radiotherapy may experience mucositis, dermatitis, dysphagia, a dry mouth, thickened saliva, or fatigue. An optimal treatment with minimal loss of functional aspects of these important organs needs thorough investigation of the therapeutic options.

Due to recent advances in therapeutic options, the survival rates of HNSCC have improved over the last two decades. However, the five-year survival rates are still poor. The overall 5-years survival for head and neck cancers is approximately 60%: 5-years survival of cancers of the larynx, oral cavity, oropharynx, and hypopharynx are respectively 70%, 62%, 48% and 33% [4]. These low survival rates are thought to be caused by the occurrence of distant metastases or locoregional recurrence due to

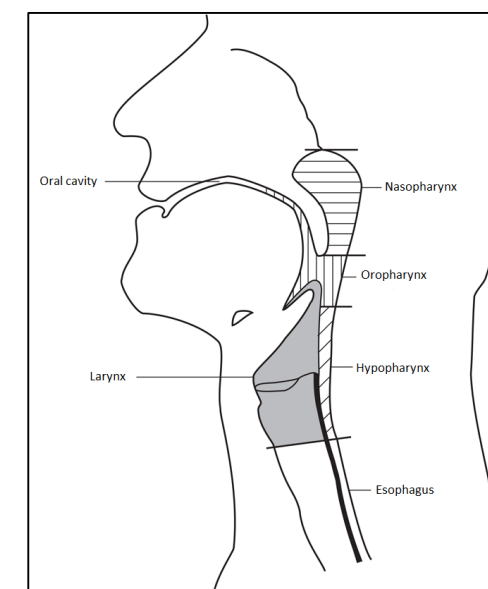


**Figure 1.** Schematic drawing of the sites and subsites in head and neck region (Figure adapted from Ridge *et al.* [7])

**Table 1.** Type and subtypes in head and neck region with preferred therapeutic approaches for each type, in accordance with the Dutch Guidelines for the treatment of HNSCC. Abbreviations; PORT: post-operative radiotherapy.

Subsites		Therapeutic approaches
Oral cavity	Lip	Preferred treatment: Surgery (on indication PORT) Alternatives: Radiotherapy, Brachytherapy or Photodynamic therapy
	Buccal mucosa	Surgery or radiotherapy (T1-2N0) Surgery with PORT (T3-4N0- and T1-4N+)
	Alveolar ridge and retromolar trigone	Preferred treatment: Surgery (on indication PORT)
	Floor of mouth	Alternatives: Radiotherapy, Brachytherapy or Photodynamic therapy
	Hard palate	Photodynamic therapy
	Anterior two-thirds of the tongue	
Nasopharynx	-	Radiotherapy (T1-2) Surgery (T3-4)
Oropharynx	Base of tongue	Preferred treatment: Radiotherapy
	Soft palate	Alternatives: surgery
	Tonsillar pillar and fossa	
Hypopharynx	-	Preferred treatment: Radiotherapy of tumor with elective radiotherapy of neck tissue both sides Alternatives: Total or partial pharyngectomy
Larynx	Supraglottis (false cords, arytenoids, epiglottis, aryepiglottic fold)	Preferred treatment: Radiotherapy Alternatives: Laser surgery or total/partial laryngectomy
	Glottis	
	Subglottis	

intrinsic or acquired treatment resistance [5, 6]. Early non-invasive monitoring of treatment response could allow clinicians to determine whether the treatment should be adjusted. This will consequently improve patients' outcome as well as patients' quality of life.

#### *Treatment of head and neck cancer*

The detection and staging of head and neck tumors include clinical examination by an experienced clinician, which is subsequently followed by further examination using (non)-invasive modalities, such as fibre optic endoscopy or examination under general anesthesia. The use of imaging modalities such as magnetic resonance imaging (MRI), computed tomography (CT), Ultrasound, and <sup>18</sup>F-fluoro-2-deoxyglucose positron emission tomography imaging (FDG-PET/CT) are used to confirm the malignancy and will further reveal the anatomical extent of the disease. Treatment plans are formulated by a multidisciplinary team and should result in maximal locoregional and distant control and survival with minimal resulting functional damage. In case of advanced disease stages, the aim of treatment is to preserve functional outcome and, at the same time, systemic control of the disease.

Treatment of advanced HNSCC tumors include surgery or radiotherapy. Several treatment strategies to improve the outcome of advanced HNSCC have been introduced, based on improved insights in the molecular interactions involved in cancer. Due to this improved understanding, the addition of chemotherapy to radiotherapy was investigated. The development of targeted drugs have led to the ability to target tumors more specifically and efficacy by combining pharmacological interventions with radiotherapy. It was shown that combination therapy not only improved the overall survival of

patients with nasopharyngeal carcinomas, but also showed improved locoregional and distant control, a higher progression-free survival rate and less cancer mortality [8]. Well known targeting agents include cetuximab, a epidermal growth factor receptor monoclonal antibody (EGFR inhibitor), EGFR tyrosine kinase inhibitors (Gefitinib), and vascular endothelial growth factor receptor (VEGF) inhibitors (Bevacizumab and Sorafenib). The mechanism of these targeting agents are reviewed elsewhere [9, 10].

Whereas clinicians can reduce the morbidity in patients with early- and locally advanced HNSCC, it has become clear that other strategies are needed to further improve advanced HNSCC control and survival. By characterization of tumors, clinicians are now able to individualize therapeutic options. Early non-invasive monitoring of treatment response in these kind of patients may avoid further side effects of treatments that are ineffective or prevent overtreatment in patients that do respond to the chosen (chemo)-radiotherapy. Monitoring treatment response may also prevent ineffective ongoing treatment, which will avoid unnecessary health care costs. Therefore, the identification of biomarkers or non-invasive imaging tools that can steer treatment decisions in the early phases of treatment are needed.

#### **Molecular pathways involved in (head and neck) cancer**

##### *Hallmarks of cancer*

Each specific tumor type that is known to date, has its own unique micro-environment in which diverse cell types can interact with each other. The heterogeneity of cancers in different patients and even within one patient makes the biology of cancer complex. It is known that most types of cancer cannot be seen as a single disease and that tumors are more than only cell masses with the ability to proliferate. In 2000, six so called 'hallmarks of cancer' were defined by Hanahan and Weinberg, characterizing the unique tumor capabilities that could describe the biology of cancer [11]. It led to an improved understanding of the functional role of several characteristics of different cells of the tumor, indicating that besides the ability to sustain chronic proliferation, tumor cells also release growth suppressors to negatively regulate chronic proliferation, can induce angiogenesis, have the capacity to resist cell death and that cell-to-cell interaction can result in local invasion and distant metastasis. New insights in tumor cell behavior resulted in an expansion of the 'hallmarks of cancer' in 2011. The ten hallmarks are illustrated in Figure 2 [12]. It goes beyond the scope of this thesis to introduce all these different types of interactions, possible targets and molecular pathways. Therefore, we refer to the article of Hanahan and Weinberg [12]. Hanahan and Weinberg also discussed the drugs that are currently being developed and investigated (or already applied in clinic) to deregulate elevated levels of receptor proteins involved in one of the cancer cell characteristics (examples depicted in Figure 2).

##### *Angiogenesis*

Angiogenesis is essential for tumor growth and metastasis. It is therefore a promising target for targeting agents to inhibit tumor progression. Angiogenesis is defined as the formation of new blood vessels from existing blood vessels. Growing tumors have the ability to initiate angiogenesis. In order to grow beyond the size of 1-2 mm, the formation of new blood vessels in a tumor is required to facilitate the supply of oxygen and nutrients, but also to dispose waste. Angiogenesis is a multi-factorial process and many of the factors involved also play a role in wound healing and embryogenesis [13]. In this multi-factorial process several events take place controlled by growth factors, cellular receptors and adhesion molecules to obtain a complex balance of both pro- and anti-angiogenic signals [14]. When a growing tumor mass results in hypoxia, this angiogenic balance is tipped to pro-angiogenesis

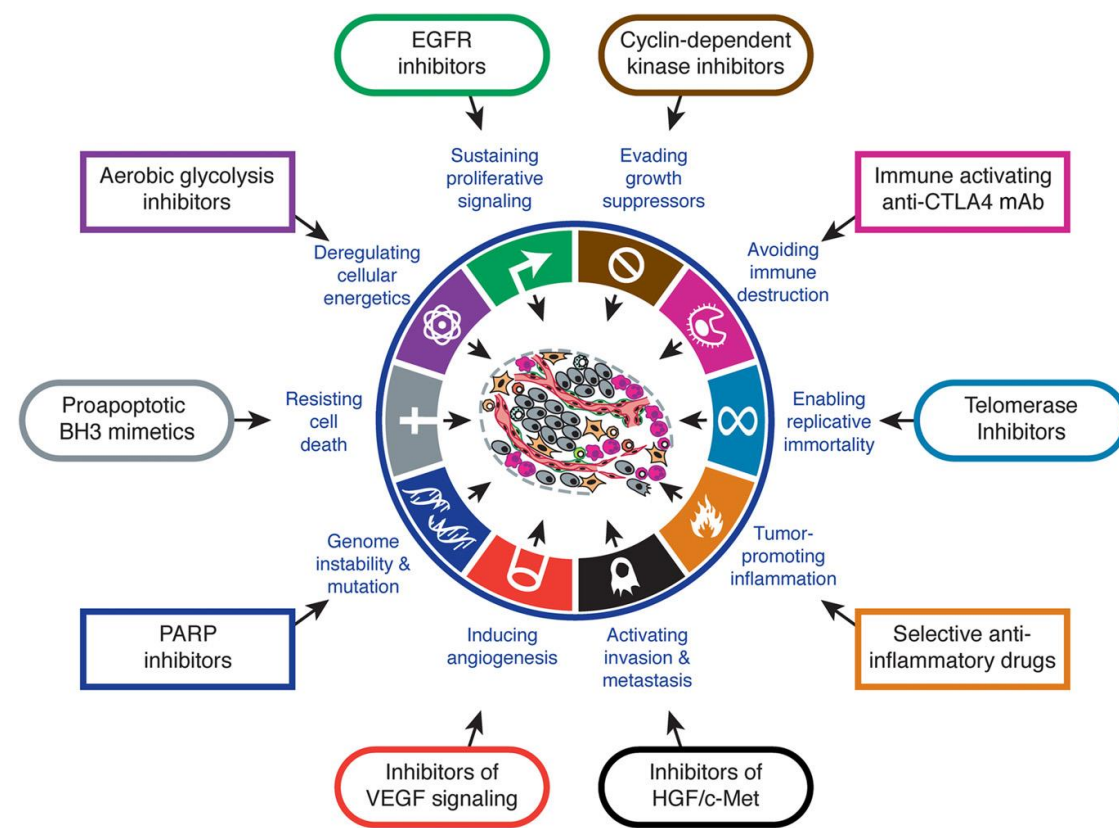


**Figure 2.** The six 'hallmarks of cancer' as defined by Hanahan and Weinberg in 2007 with the addition of the four new hallmarks as defined in 2011 (deregulation of cellular energetics, avoiding immune destruction, genome instability and mutation, and tumor-promoting inflammation), together with possible drugs that are currently being developed and investigated to target one of the defined 'hallmarks of cancer'. Figure obtained from Hanahan *et al.* [12].

and a cascade of events is initiated. This so-called 'angiogenic switch' [15] includes the expression of hypoxia inducible factor HIF1- $\alpha$ , activation of endothelial cells and release of cytokines and several growth factors, such as vascular endothelial growth factor (VEGF-A), carbonic anhydrase IX (CAIX), or transforming growth factor- $\alpha$  (TGF- $\alpha$ ), into the microenvironment [13, 16]. The cascade of events in angiogenesis is illustrated in Figure 3.

#### Process of angiogenesis

Angiogenesis is regulated by several angiogenic factors, including proteins, cytokines, integrins, and the extracellular matrix. Cells themselves also regulate the process of angiogenesis. One of the first steps in blood vessel growth is the detachment of activated endothelial cells from their neighboring cells. They subsequently sprout towards the pro-angiogenic factors, including cytokines and several growth factors, that are released around the site of the tumor [6]. One particular set of growth factors released by activated endothelial cells are the matrix metalloproteases (MMP), which are able to degrade the basement membrane, a membrane that is part of the vessel extracellular matrix (ECM). This process is then followed by the overexpression of integrins on the activated endothelial cells [16]. The expression of several integrins on the endothelial cells allows the endothelial cell to interact with ECM proteins such as collagen, vitronectin and fibronectin. This results in migration of tumor cells by facilitating invasion and movement across blood vessels through the release of cytokines [5]. Once the endothelial cells are transformed to solid cords and the vessel lumen has been developed, the so-called immature vasculature

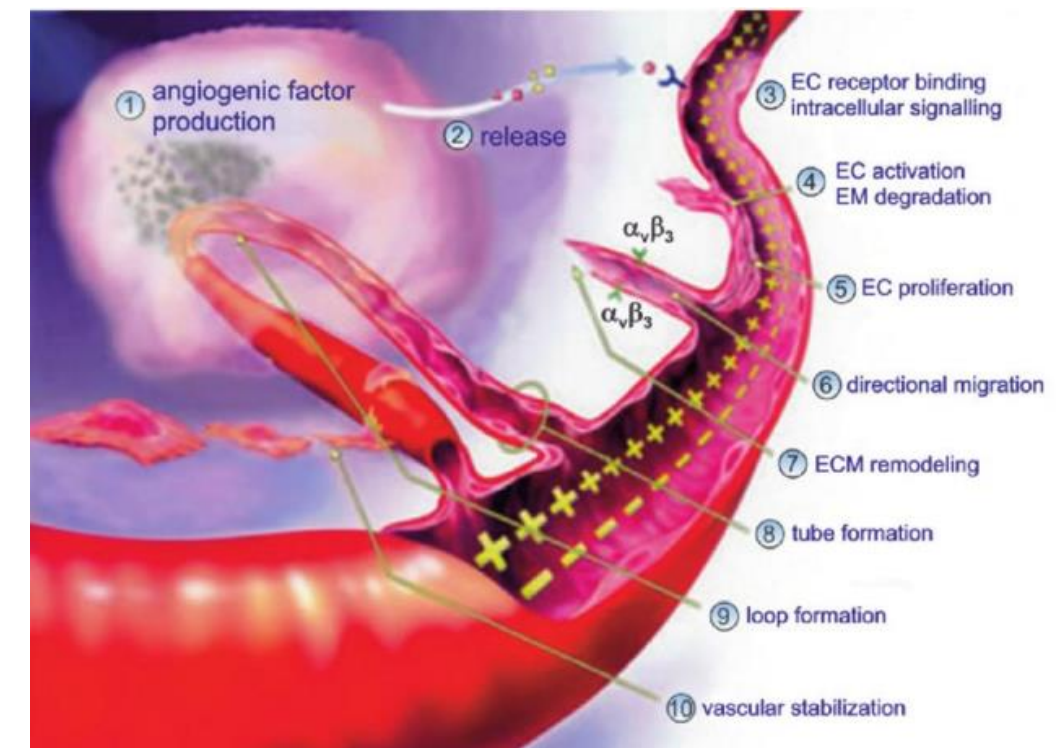


**Figure 3.** The cascade of events in angiogenesis. The numbers indicate the different steps in angiogenesis, starting with the 'angiogenic switch'. After release of angiogenic factors, endothelial cells are activated and  $\alpha_v\beta_3$  integrin is expressed on the endothelial cells, subsequently followed by the sprouting of new blood vessels towards tumor tissue. Figure obtained from [17]. Initial source is The Angiogenesis Foundation ([www.angio.org](http://www.angio.org)).

undergoes remodeling and become mature vessels. However, these blood vessels are typically abnormal compared to blood vessels formed by vasculogenesis, showing porous basement membranes, resulting in a high permeability, erratic blood flow, leaky vessels, and micro hemorrhaging [18].

#### $\alpha_v\beta_3$ integrin expression

Integrins are transmembrane proteins with two non-covalently bound subunits. Integrins are involved in growth, survival, adhesion, and in motility of cells [19]. They serve as a receptor for interactions of the endothelial cells with the ECM. Eighteen  $\alpha$ - and eight  $\beta$ -subunits were discovered, forming at least twenty four different integrins, which are the result of the combination of one of both subunits [20]. One of the integrins that has been discovered and is known to be overexpressed on activated endothelial cells is  $\alpha_v\beta_3$  integrin. Normally, integrins present on the surface of the endothelial cells are inactive and cannot bind ECM proteins. However, if intracellular signaling pathways are activated, the integrins change in active binding sites, allowing the integrin to bind specific ECM molecules. These ECM molecules are recognized because they express the arginine-glycine-aspartic acid sequence (RGD). The RGD sequence is present on many ECM and some secreted proteins, such as fibronectin, vitronectin, fibrinogen, laminin, collagen, Von Willebrand factor, osteopontin, and trombospondin. The  $\alpha_v\beta_3$  integrin bind to the RGD sequence of the ECM proteins. Once integrins are activated, they are able to activate intracellular signaling pathways that allow gene-expression changes. This will then lead to cell growth, survival, adhesion, or cell motility. Since  $\alpha_v\beta_3$  integrin is significantly up-regulated on activated endothelial tumor cells and is not expressed on quiescent endothelial cells, it is considered to be an important biomarker of angiogenesis.

### Imaging of $\alpha_v\beta_3$ integrin expression

With molecular imaging it is feasible to non-invasively visualize, characterize, and quantify biological processes at a molecular level. Positron Emission Tomography (PET) and Single-Photon Emission Computed Tomography (SPECT) are two molecular imaging techniques that allow the visualization of molecular pathways using radiolabeled proteins, protein fragments, or metabolites. Radiotracers are intravenously administered and accumulate in tissue according to the expression of molecular targets, metabolism, and corresponding uptake pattern of that protein or protein fragment.

Different strategies were used to optimize  $\alpha_v\beta_3$  integrin targeting for PET and SPECT imaging. Several radiolabeled RGD peptides targeting  $\alpha_v\beta_3$  integrin have been developed and tested in preclinical and clinical trials [21, 22]. The RGD-based radiotracers that were used in clinical studies, includes the monomers  $^{18}\text{F}$ -Galacto-RGD [23-29],  $^{18}\text{F}$ -Fluciclatide [30],  $^{18}\text{F}$ -RGD-K5 [31], and  $^{68}\text{Ga}$ -NOTA-RGD [32], and the dimeric compounds  $^{18}\text{F}$ -FPPRGD<sub>2</sub> [33-36],  $^{18}\text{F}$ -FPRGD<sub>2</sub> [37, 38],  $^{18}\text{F}$ -Alfatide [39],  $^{18}\text{F}$ -Alfatide II [40, 41], and  $^{68}\text{Ga}$ -NOTA-PRGD<sub>2</sub> [42]. These RGD-based radiotracers showed similar pharmacokinetics and dosimetric profiles (ranging from 10-40  $\mu\text{Sv}/\text{MBq}$ ). The conducted clinical trials focused on the feasibility and the evaluation of safety profiles in patients with several types of cancer, including lung cancer [27, 32, 33, 35, 39, 42, 43], head and neck cancer [23, 25-27], breast cancer [25-28, 30, 34, 35, 44], melanomas [24-26], sarcomas [24], renal cell cancer [24, 27, 38], rectal cancers [27, 37], and glioblastoma multiforme (GBM) [25, 33, 35, 45, 46]. Furthermore, some studies examined the potential role of imaging  $\alpha_v\beta_3$  integrin expression as biomarker of response to therapy [33, 37, 47]. Zhang *et al.* found that  $^{18}\text{F}$ -AlF-NOTA-PRGD<sub>2</sub> PET/CT was predictive of treatment sensitivity to concurrent chemoradiotherapy [47]. Imaging  $\alpha_v\beta_3$  integrin expression can steer treatment decisions to improve patient outcome or minimize side effects, but will need further investigation.

#### $^{68}\text{Ga}$ -DOTA-RGD<sub>2</sub> PET/CT

An attractive radiotracer that has been developed to image  $\alpha_v\beta_3$  integrin is  $^{68}\text{Ga}$ -labeled DOTA-E-[c(RGDfK)]<sub>2</sub>, further designated as  $^{68}\text{Ga}$ -DOTA-RGD<sub>2</sub>. This is a cyclic dimeric version of RGD where two RGD monomers are connected via a glutamic acid residue. Labeling DOTA-RGD<sub>2</sub> is a simple and fast procedure and can be performed in an automated fashion. With subcutaneously growing SK-RC-52 renal cell cancer xenografts, the *in vitro* and *in vivo*  $\alpha_v\beta_3$  targeting properties of  $^{68}\text{Ga}$ - and  $^{111}\text{In}$ -labeled DOTA-RGD<sub>2</sub> were determined in mice [48, 49]. These preclinical studies proved that the tumor uptake of dimeric RGD peptides with two binding sites for  $\alpha_v\beta_3$  integrin is higher than the tumor uptake of RGD monomers with one binding site for  $\alpha_v\beta_3$  integrin, due to enhanced affinity for  $\alpha_v\beta_3$  integrin [48, 49]. These experiments proved the *in vivo*  $\alpha_v\beta_3$  integrin targeting possibilities of  $^{68}\text{Ga}$ -DOTA-RGD<sub>2</sub>, making them a potential radiotracer to image angiogenesis in different tumor models. The imaging potential of DOTA-RGD<sub>2</sub> to visualize  $\alpha_v\beta_3$  integrin expression in HNSCC was investigated in a preclinical study using thirteen patient-derived HNSCC xenografts of BALB/c nude mice [50]. The microSPECT/CT images of mice injected with  $^{111}\text{In}$ -DOTA-RGD<sub>2</sub> showed clear uptake of the tracer at the periphery of the tumors. *In vivo* blocking of  $\alpha_v\beta_3$  integrin with a blocking dose of DOTA-RGD<sub>2</sub> led to decreased visualization of  $^{111}\text{In}$ -labeled DOTA-RGD<sub>2</sub> within the tumor, indicating that the uptake of the tracer in the tumor was integrin  $\alpha_v\beta_3$  mediated (Figure 4). Furthermore, tumor and vascular  $\alpha_v\beta_3$  integrin expression on the tumor tissue was determined using immunohistochemical staining profiles of the tumor tissue. The immunohistochemical staining confirmed the sole expression of  $\alpha_v\beta_3$  integrin on neovascular structures within the tumor. This experiment proved that  $^{111}\text{In}$ -DOTA-RGD<sub>2</sub> allows specific visualization of angiogenesis in head and neck tumors. So far, these experiments showed the potential of imaging

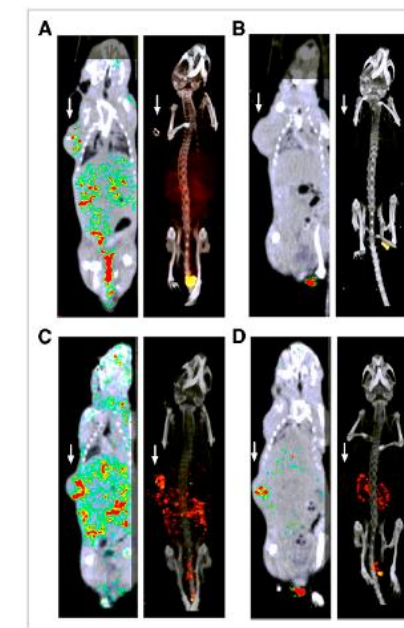


**Figure 4.** Fused SPECT/CT scans (1 hour post injection) of mice with subcutaneous tumor xenografts on right flank (white arrows). A and C: mice injected with  $^{111}\text{In}$ -DOTA-RGD<sub>2</sub> showing tracer uptake within tumor tissue. B and D: mice injected with  $^{111}\text{In}$ -DOTA-RGD<sub>2</sub> and cold excess showing reduced tracer uptake in tumor and non-tumor tissue. Figure obtained from Terry *et al.* [50].

$\alpha_v\beta_3$  integrin expression using  $^{68}\text{Ga}$  and  $^{111}\text{In}$ -labeled DOTA-RGD<sub>2</sub>. In a subsequent experiment, the effect of local irradiation on the *in vivo* uptake of  $^{111}\text{In}$ -DOTA-RGD<sub>2</sub> in the tumor was determined up to 3 weeks after irradiation [51]. The tumor models showed a decreased uptake of DOTA-RGD<sub>2</sub> after tumor irradiation, indicating that  $^{111}\text{In}$ -DOTA-RGD<sub>2</sub> can be used to monitor responses after radiotherapy. Using  $^{68}\text{Ga}$ -DOTA-RGD<sub>2</sub> PET/CT as an imaging biomarker of angiogenesis will be feasible. However, the real potential and implementation in clinical practice need to be confirmed.

#### Research questions

Preclinical studies showed that  $^{68}\text{Ga}$ -DOTA-RGD<sub>2</sub> can image  $\alpha_v\beta_3$  integrin expression on newly formed endothelial cells in HNSCC. It was also shown that this radiolabeled RGD peptide can serve as a tool to monitor angiogenic responses after radiotherapy. **The aim** of this project is to translate these preclinical results into a clinical study in HNSCC patients.

The **main question** to be answered in this thesis is: is it feasible to use  $^{68}\text{Ga}$ -DOTA-RGD<sub>2</sub> PET/CT to image angiogenesis in head and neck squamous cell carcinomas by targeting  $\alpha_v\beta_3$  integrin expression? Therefore, the following sub questions are formulated:

1. Does the  $^{68}\text{Ga}$ -labeled radiotracer DOTA-RGD<sub>2</sub> show favorable *in vitro* and *in vivo* targeting characteristics compared to the currently available 'improved' RGD-based radiotracers?
2. Evaluate the safety of injection of  $^{68}\text{Ga}$ -DOTA-RGD<sub>2</sub> in patients;
3. Determine the pharmacokinetic and pharmacodynamic behavior of  $^{68}\text{Ga}$ -DOTA-RGD<sub>2</sub> in human;
4. Determine the biodistribution pattern of  $^{68}\text{Ga}$ -DOTA-RGD<sub>2</sub>;
5. Determine the correlation between the  $^{68}\text{Ga}$ -DOTA-RGD<sub>2</sub> PET/CT findings and the  $\alpha_v\beta_3$  integrin expression on tumor tissue.

### Outline of this thesis

**Chapter 2** provides an overview about the current status of four potential PET tracers to image angiogenesis. All four radiotracers are subsequently labeled with Gallium-68, and the affinity of each tracer is determined in a solid phase competitive binding assay. Then, the *in vivo*  $\alpha_v\beta_3$  integrin targeting characteristics of the four tracers are determined in mice with subcutaneously growing  $\alpha_v\beta_3$  integrin-expressing tumors. The aim of these *in vitro* and *in vivo* experiments is to describe the  $\alpha_v\beta_3$  integrin targeting characteristics of the four radiotracers when a head-to-head comparison under standardized conditions is performed.

The dimeric RGD-based radiotracer,  $^{68}\text{Ga}$ -DOTA-RGD<sub>2</sub>, is an attractive RGD-based radiotracer to image angiogenesis, because it can be radiolabeled very rapidly, efficiently, in an automated fashion, and according to the Good Manufacture Practice Guidelines. In **Chapter 3** the methodological set-up to study the feasibility of  $^{68}\text{Ga}$ -DOTA-RGD<sub>2</sub> PET/CT imaging in HNSCC patients is given followed by the preliminary results of the ongoing feasibility study. In that clinical study, HNSCC patients undergo three static whole body  $^{68}\text{Ga}$ -DOTA-RGD<sub>2</sub> PET/CT scans prior to their surgical treatment.

The last chapter of this thesis (**Chapter 4**) provides a general discussion including future perspectives of the potential of  $^{68}\text{Ga}$ -DOTA-RGD<sub>2</sub> PET/CT in therapy response monitoring in HNSCC patients.

## Chapter 2: A direct comparison of four $^{68}\text{Ga}$ -labeled RGD peptides to image $\alpha_v\beta_3$ integrin expression in mice with tumor xenografts

### Introduction

Non-invasive imaging of tumor characteristics using molecular imaging techniques, such as SPECT and PET, requires radiolabeled vectors (e.g. peptides or other molecules). In case of radiolabeled peptides, the procedure of radiolabeling should not affect the receptor binding affinity of the peptide or affect the *in vivo* behavior of the radiolabeled peptide. Various techniques have been developed that enable efficient labeling of peptides with radionuclides such as  $^{99\text{m}}\text{Tc}$ ,  $^{123}\text{I}$ ,  $^{111}\text{In}$ ,  $^{64}\text{Cu}$ ,  $^{18}\text{F}$ , and  $^{68}\text{Ga}$  [21, 52]. To be able to conjugate peptides with radiometals, a functional chelator is required. The chemical properties of the bond between chelator, peptide and radionuclide is critical for maintaining the biological and receptor properties of the peptide. With the availability of GMP-compliant  $^{68}\text{Ge}/^{68}\text{Ga}$  generators, and the excellent physical characteristics of  $^{68}\text{Ga}$  (short half-life (68 minutes) and high positron yield (89%)),  $^{68}\text{Ga}$ -labeled peptides are increasingly considered to be potential tracers for PET imaging. A series of chelators for labeling RGD-based peptides with  $^{68}\text{Ga}$  have been developed, such as 1,4,7,10-tetraazacyclododecane-N',N'',N''',N''''-tetraacetic acid (DOTA), DOTA derivative analogs (DOTAGA), 1,4,7-triazacyclononane-triacetic acid (NOTA), a NOTA-derivatized chelating system (NODAGA), triazacyclononane-phosphinate (TRAP), and Fusarinine-C (FSC) [53, 54]. Major efforts have been made in developing stable  $^{68}\text{Ga}$ -labeled targeting peptides that have a high affinity for  $\alpha_v\beta_3$  integrin. These targeting agents are produced using different labeling procedures, with varying preparation time, radiochemical yield, and radiochemical purity [21]. However, most of the newly developed tracers can be radiolabeled very efficiently (>90%), rapidly (<30 minutes) and in a fully automated GMP compliant manner, which makes them suitable for clinical studies.

Multimerization of RGD-based peptides was considered as another technique to further improve binding affinity for  $\alpha_v\beta_3$  integrin. Multimeric RGD-based radiotracers have more than one RGD binding site at the surface. Due to an increased number of binding sites within one molecule, a lower tracer concentration is needed to achieve equal tracer uptake. After it was revealed that dimeric, trimeric, and tetrameric RGD analogues showed enhanced accumulation in  $\alpha_v\beta_3$  integrin expressing tumors compared to their monomeric counterparts [48, 49, 55, 56], several multimeric RGD-based peptides have been developed. Although the DOTA-conjugated tetrameric RGD-based peptide showed enhanced affinity for  $\alpha_v\beta_3$  integrin, it also showed significantly higher kidney uptake, making it a less attractive radiotracer in clinical practice [49]. The dimeric RGD peptide,  $^{68}\text{Ga}$ -DOTA-RGD<sub>2</sub>, showed a favorable biodistribution [48], and was therefore introduced in clinical practice.

Today, a large variety of other multimeric radiolabeled RGD peptides with other chelators are described in literature and have been studied in a preclinical setting [21]. Some of these radiotracers have been introduced in the clinic [22]. The fact that only a few of these tracers have been used for clinical imaging is mainly due to the extensive mandatory regulatory requirements needed to introduce radiotracers into clinical practice. While these radiotracers all allow imaging of  $\alpha_v\beta_3$  integrin expression using PET/CT and show sufficient tumor-to-tissue ratios, the results described in literature do not allow direct comparison of these tracers due to differences in the tumor models and imaging methods used. To be able to compare the *in vitro* and *in vivo* image characteristics of different  $^{68}\text{Ga}$ -labeled RGD-based peptides, the radiolabeled tracers need to be compared in the same animal model and using the same experimental set-up. Therefore, the aim of this study was to compare the *in vitro* and *in vivo*  $\alpha_v\beta_3$

targeting characteristics of  $^{68}\text{Ga}$ -DOTA-RGD<sub>2</sub> under standardized conditions with three other promising multimeric cyclic RGD-based radiotracers:  $^{68}\text{Ga}$ -TRAP-RGD<sub>3</sub>,  $^{68}\text{Ga}$ -FSC-RGD<sub>3</sub>, and  $^{68}\text{Ga}$ -THP-RGD<sub>3</sub>, [49, 53, 54, 57-61]. First, the four radiotracers are introduced.

#### $^{68}\text{Ga}$ -DOTA-RGD<sub>2</sub>

One of the most widely used chelators is DOTA, because it forms a stable complex with  $^{68}\text{Ga}$  *in vivo*. Furthermore, it was shown that DOTA is also suitable for a wide range of beta-emitters such as Lutetium-177 ( $^{177}\text{Lu}$ ) and yttrium-90 ( $^{90}\text{Y}$ ), making it an attractive chelator for therapeutic applications. However, a disadvantage of DOTA is that high labeling efficiencies can only be obtained when the radiolabeling procedure is performed at high temperatures (80-120 °C), which may change the structure and with this the receptor binding properties of the peptide used.

Radio-labeling of RGD peptides with  $^{68}\text{Ga}$  and with DOTA as a chelator is a simple and fast procedure (<30 min), and can be performed in an automated fashion. The two RGD monomers of  $^{68}\text{Ga}$ -DOTA-RGD<sub>2</sub> are connected via a glutamic acid residue. The chemical structure of the DOTA-conjugated dimeric RGD peptide is given in Figure 5. In our preclinical studies, it was shown that this PET-tracer is stable over time, is predominantly cleared via the kidneys, and can be used to visualize  $\alpha_v\beta_3$  integrin expression with tumor uptake values ranging from  $1.37 \pm 0.37$  %ID/g to  $7.11 \pm 0.67$  %ID/g [49, 50].

#### $^{68}\text{Ga}$ -TRAP-RGD<sub>3</sub>

Advances in labeling strategies have shown that the use of other chelators may show improved  $^{68}\text{Ga}$ -labeling properties when compared to DOTA. In  $^{68}\text{Ga}$ -TRAP-RGD<sub>3</sub>, the chemical phosphinic acid group allows direct conjugation of three RGD peptides. This results in a reduced amount of peptide needed to achieve equal percentage binding, due to more specific binding of RGD [53, 60]. This makes TRAP a suitable multimeric RGD peptide (the chemical structure is given in Figure 5). Another advantage of TRAP as a chelator is that the labeling of TRAP-RGD<sub>3</sub> to  $^{68}\text{Ga}$ , yielding  $^{68}\text{Ga}$ -TRAP-RGD<sub>3</sub>, can be performed at room temperature and over a broad pH range. In a study conducted by Notni *et al.* and Haubner *et al.* [60, 62], the *in vivo* integrin-targeting properties of  $^{68}\text{Ga}$ -TRAP-RGD<sub>3</sub> were compared with the clinically available radiotracer  $^{18}\text{F}$ -Galacto-RGD and a monomeric  $^{68}\text{Ga}$ -labeled RGD peptide,  $^{68}\text{Ga}$ -NODAGA-RGD.  $^{68}\text{Ga}$ -TRAP-RGD<sub>3</sub> showed a 7.6 and 7.3 fold higher affinity to  $\alpha_v\beta_3$  integrin expression compared to the  $^{18}\text{F}$ -labeled and  $^{68}\text{Ga}$ -labeled monomers respectively [60]. Furthermore, the *in vivo* experiments showed tracer accumulation in an  $\alpha_v\beta_3$  integrin expressing melanoma tumor model of  $6.08 \pm 0.63$  %ID/g,  $1.45 \pm 0.11$  %ID/g, and  $1.35 \pm 0.53$  %ID/g respectively [60].

#### $^{68}\text{Ga}$ -FSC-RGD<sub>3</sub>

$^{68}\text{Ga}$ -FSC-RGD<sub>3</sub> is another radiolabeled RGD-based peptide that shows promising  $^{68}\text{Ga}$  labeling properties in a labeling procedure of only 15 minutes. FSC is a cyclic hydroxamate siderophore with three primary amino groups that allows conjugation of three RGD peptides (see Figure 5). One of the benefits of the chelator of this radiotracer is the conjugation and labeling at room temperature, resulting in high radiochemical purity [54, 59]. Specific activities ranging from 4 to 200 MBq/nmol were reached. Tumor uptake values in a Melanoma M21 xenograft models showed tracer accumulation of  $3.69 \pm 0.94$  [59]. Overall, in PET/CT imaging of xenograft models they showed comparable tumor-to-muscle ratios as observed in studies with the radiotracers  $^{68}\text{Ga}$ -TRAP-RGD<sub>3</sub> and  $^{68}\text{Ga}$ -NODAGA-RGD:  $7.3 \pm 0.8$ ,  $6.4 \pm 1.9$ , and  $6.1 \pm 3.5$  respectively [59].

#### $^{68}\text{Ga}$ -THP-RGD<sub>3</sub>

Most recently, a radiotracer,  $^{68}\text{Ga}$ -THP-RGD<sub>3</sub>, has been developed in order to simplify the radiopharmaceutical preparation of RGD-based radiotracers [61]. This peptide consists of a thiocyanate group and three 1,6-dimethyl-3-hydroxypyridin-4-one groups which allows radiolabeling of  $^{68}\text{Ga}$  and three RGD peptides [57, 58]. This radiotracer allows fast labeling procedures (<5 minutes) at room temperature, without acidic conditions (that is required for DOTA conjugation). Tumor uptake values of  $4.3 \pm 0.5$  %ID/g were seen in glioblastoma tumor xenografts (U87MG) 1 hour after injection.

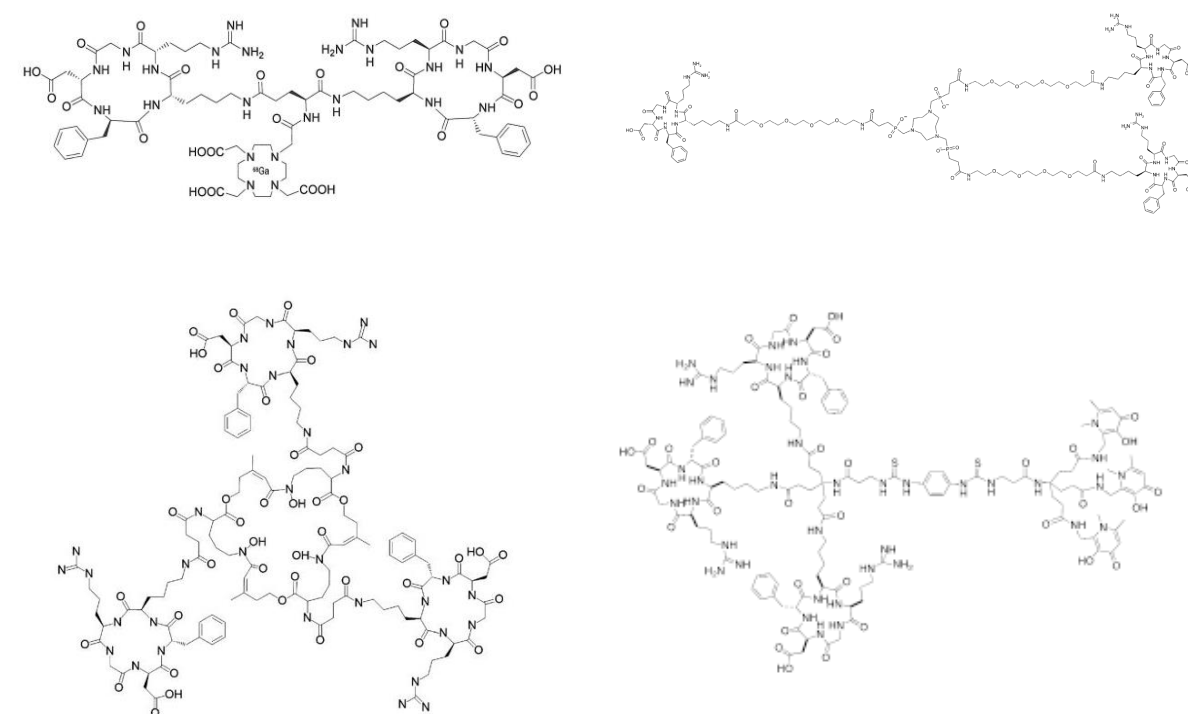


Figure 5. Chemical structures of  $^{68}\text{Ga}$ -DOTA-RGD<sub>2</sub> (upper left),  $^{68}\text{Ga}$ -TRAP-RGD<sub>3</sub> (upper right),  $^{68}\text{Ga}$ -FSC-RGD<sub>3</sub> (lower left), and  $^{68}\text{Ga}$ -THP-RGD<sub>3</sub> (lower right).

## Materials and method

### Radiolabeling and quality control

#### Radiolabeling of $^{68}\text{Ga}$ -DOTA-RGD<sub>2</sub>

DOTA-RGD<sub>2</sub> was labeled with  $^{68}\text{GaCl}_3$  eluted from a  $^{68}\text{Ge}/^{68}\text{Ga}$  generator using 0.1 M HCl. Three 1-ml fractions were collected.  $^{68}\text{Ga}$ -labeled DOTA-RGD<sub>2</sub> was prepared by adding 700  $\mu\text{l}$   $^{68}\text{Ga}$  eluted from the generator (186 MBq) to 88  $\mu\text{l}$  1M HEPES solution, pH 3.8. Then, 6  $\mu\text{l}$  (0.5 nmol) of the peptide dissolved (1  $\mu\text{g}/\mu\text{l}$ ) in 0.25M ammonium acetate, pH 5.5 was added. After 20 minutes at 95°C, the eluate was diluted with 200  $\mu\text{l}$  phosphate buffered saline-bovine serum albumin (PBS/BSA), 10  $\mu\text{l}$  phosphate, 5  $\mu\text{l}$  5M NaOH, 1000  $\mu\text{l}$  10x PBS, and 91  $\mu\text{l}$  EDTA.

For the excess cold experiment, a new labeling procedure has been performed using the same labeling procedure as described above. After 20 minutes at 95°C,  $^{68}\text{Ga}$ -DOTA-RGD<sub>2</sub> was further purified on an Oasis® Hydrophilic-Lipophilic-Balanced (HLB) (1 cm<sup>3</sup>, 30 mg) cartridge. After applying the sample on the cartridge, the cartridge was washed three times with 1 ml H<sub>2</sub>O and eluted with 200  $\mu\text{l}$  25% EtOH in

Table 2. Tracer characteristics and results from previous obtained preclinical experiments

	<sup>68</sup> Ga-DOTA-RGD <sub>2</sub> [49]	<sup>68</sup> Ga-TRAP-RGD <sub>3</sub> [53, 60]	<sup>68</sup> Ga-FSC-RGD <sub>3</sub> [54, 59]	<sup>68</sup> Ga-THP-RGD <sub>3</sub> [57, 58, 61]
<b>Tracer characteristics</b>				
Chelator	1,4,7,10-tetraazacyclododecane-N',N'',N''',N''''-tetraacetic acid	1,4,7-triazacyclononane-1,4,7-tris[(2-carboxyethyl)-methylphenosphinic acid]	fusarinine-C	Tris(hydroxyl-pyridinone)
Specific activity	11.2 MBq/nmol	800 - 1000 MBq/nmol	4 - 200 MBq/nmol	8-9 MBq/nmol
Number of RGDs	2	3	3	3
Lipophilicity (octanol/water partition coefficient)	-4.04 ± 0.15	-3.90 ± 0.10	-3.6	N/A
Binding affinity	8.99 ± 1.20 nM for Ga(III)-DOTA-RGD <sub>2</sub>	7.36 ± 0.05 nM for Ga(III)-TRAP-RGD <sub>3</sub>	1.8 ± 0.6 nM for <sup>68</sup> Ga-FSC-RGD <sub>3</sub>	N/A
Molecular weight	1704.8 g/L	3145.0 g/L	2782.3 g/L	3720.6 g/L
<b>Mouse model used in <i>in vivo</i> studies</b>				
Injected dose	0.89 nmol	NA	0.4 µg (0.14 nmol)	50 µg (13 nmol)
Injected amount of activity	10 MBq	7-10 MBq	1 MBq	18-33 MBq
Mouse model	Balb/c nude mice, female	CD-1 nude mice, female	Balb/c nude mice, female	Balb/c nude mice, female
Tumor model	Renal cell carcinoma SK-RC-52	Melanoma M21 and M21L	Melanoma M21	Glioblastoma U87MG
Tracer uptake in tumor tissue	5.24 ± 0.27 %ID/g	6.08 ± 0.63 %ID/g	3.69 ± 0.94 %ID/g	4.3 ± 0.5 %ID/g
Tumor-to-blood ratio	N/A	19.4 ± 9.1	6.4 ± 2.5	N/A

H<sub>2</sub>O (v/v). 85.5 µl (5 mg/ml) DOTA-RGD<sub>2</sub> excess cold was added, followed by 660.5 µl PBS/BSA, 150 µl 10x PBS, 4 µl 5M NaOH.

#### Radiolabeling of <sup>68</sup>Ga-TRAP-RGD<sub>3</sub>

TRAP-RGD<sub>3</sub> was labeled with <sup>68</sup>GaCl<sub>3</sub> eluted from a <sup>68</sup>Ge/<sup>68</sup>Ga generator using 0.1M HCl. Three 1-ml fractions were collected and a small amount of the second fraction was used for labeling the peptide. <sup>68</sup>Ga-labeled TRAP-RGD<sub>3</sub> was prepared by adding 700 µl <sup>68</sup>Ga eluted from the generator (142 MBq) to 88 µl 1 M HEPES, pH 3.8, solution. Then, 11 µl (0.5 nmol) of the peptide (1 µg/µl) was added. After 5 minutes at 95°C, the eluate was diluted with 200 µl 10x PBS, 10 µl phosphate, 5 µl 5M NaOH, 1000 µl PBS/BSA, 85 µl EDTA. Followed by 5 µl Polysorbate80 (TWEEN).

For the excess cold experiment, the same labeling method was used, but after 5 minutes at 95°C, 85.5 µl (5 mg/ml, 50 nmol) unlabeled DOTA-RGD<sub>2</sub> was added, followed by 660.5 µl PBS/BSA, 150 µl 10x PBS, 4 µl 5M NaOH.

#### Radiolabeling of <sup>68</sup>Ga-FSC-RGD<sub>3</sub>

FSC-RGD<sub>3</sub> was labeled with <sup>68</sup>GaCl<sub>3</sub> eluted from a <sup>68</sup>Ge/<sup>68</sup>Ga generator using 0.1M HCl. 750 µl of the second fraction (141 MBq) was used for labeling the peptide. <sup>68</sup>Ga-labeled FSC-RGD<sub>3</sub> was prepared by adding the <sup>68</sup>Ga-eluate to a dilution of 150 µl NaOAc solution pH 5 (sodium acetate) and 9.7 µl (0.5 nmol) of the peptide (1 µg/µl) in an Eppendorf LoBind tube. After 15 minutes at room temperature, the eluate was further diluted with 1000 µl PBS, 5 µl 5M NaOH, 200 µl 10x PBS/BSA, 85 µl EDTA, and 5 µl Polysorbate80 (TWEEN).

For the excess cold experiment the labeling procedure as described above was followed by adding 86 µl (5 mg/ml, 50 nmol) DOTA-RGD<sub>2</sub> excess cold, 565 µl PBS/BSA, 150 µl 10x PBS, 3 µl 5M NaOH to the <sup>68</sup>Ga-labeled FSC-RGD<sub>3</sub> (650 µl).

#### Radiolabeling of <sup>68</sup>Ga-THP-RGD<sub>3</sub>

For the first labeling, THP-RGD<sub>3</sub> was labeled with <sup>68</sup>GaCl<sub>3</sub> eluted from a <sup>68</sup>Ge/<sup>68</sup>Ga generator using 0.1M HCl. Three fractions, each of 1 ml, were collected and measured. The second fraction (750 µl) was used for labeling the THP-RGD<sub>3</sub> peptide. 150 µl NaOAc pH 5 was added to the <sup>68</sup>Ga-eluate. Thereafter, 13 µl (0.5 nmol) THP-RGD<sub>3</sub> was added. 202 µl 10x PBS, 900 µl PBS, and 85 µl EDTA was added to the solution containing <sup>68</sup>Ga-THP-RGD<sub>3</sub>.

For the excess cold experiment the labeling procedure as described above was followed. 86 µl (50nmol) DOTA-RGD<sub>2</sub> excess cold, 116 µl 10x PBS, 900 µl PBS, and 85 µl EDTA was added to the solution containing <sup>68</sup>Ga-labeled THP-RGD<sub>3</sub>.

#### Quality control

Before the start of the experiment, the radiochemical purity of each labeling was determined by instant thin-layer chromatography (ITLC) and reversed-phase high-performance liquid chromatography (RP-HPLC).

For <sup>68</sup>Ga-DOTA-RGD<sub>2</sub> and <sup>68</sup>Ga-TRAP-RGD<sub>3</sub>, ITLC analysis was performed using 0.1M CH<sub>3</sub>COONH<sub>4</sub>/0.1M EDTA (1:1 v/v) as mobile phase I and 0.25M CH<sub>3</sub>COONH<sub>4</sub>/MeOH (1:1 v/v) as mobile phase II. For <sup>68</sup>Ga-

FSC-RGD<sub>3</sub> mobile phase I was: 0.1M citrate pH5.0 and mobile phase II: 0.1M citrate/MeOH (1:1 v/v). For <sup>68</sup>Ga-THP-RGD<sub>3</sub>, three mobile phases were performed. Mobile phase I: 0.1M citrate/MeOH (1:1 v/v), mobile phase II: 0.1M CH<sub>3</sub>COONH<sub>4</sub>/0.1M EDTA (1:1 v/v), and mobile phase III: 0.25M CH<sub>3</sub>COONH<sub>4</sub>/MeOH (1:1 v/v). The strips were analyzed using a Fujifilm BAS-1800II Scanner (Fuji Photo Film Co., Tokyo, Japan) and Aida Software (version 4.21, Raytest GmbH, Straubenhardt, Germany).

The quality control by RP-HPLC was performed using the Agilent 1100 system (Agilent Technologies, Palo Alto, CA, USA) with a C18 column (RX-C18, 4.6×250 mm, Zorbax) eluted with a gradient mobile phase and two buffers (buffer A: 0.1% trifluoroacetic acid (TFA) in H<sub>2</sub>O, buffer B: 0.1% TFA in acetonitrile at 1 ml/min). The first gradient was 0–5 minutes with 100% to 97% buffer A, 5–15 minutes 97% buffer A to 0% buffer A. The radioactivity of the eluate was monitored using an in-line NaI radiodetector. Elution profiles were analyzed using Gabi Star software (version 4.8, Raytest GmbH, Straubenhardt, Germany).

#### Solid-phase $\alpha_v\beta_3$ integrin binding assay

The affinity of DOTA-RGD<sub>2</sub>, TRAP-RGD<sub>3</sub>, FSC-RGD<sub>3</sub>, and THP-RGD<sub>3</sub> for binding  $\alpha_v\beta_3$  integrin was determined using a solid-phase competitive binding assay. First, three buffers were made:

1. the coating buffer was a solution of 25mM Tris-HCl, pH7.4, 150mM NaCl, 1mM CaCl<sub>2</sub>, 0.5mM MgCl<sub>2</sub> and 1mM MnCl<sub>2</sub>;
2. the binding buffer was a solution of 0.1% bovine serum albumin (BSA) in coating buffer;
3. the blocking buffer was a solution of 1% BSA in coating buffer.

Each compound was dissolved in binding buffer (10.23  $\mu$ g/ml DOTA-RGD<sub>2</sub>, 18.87  $\mu$ g/ml TRAP-RGD<sub>3</sub>, 16.69  $\mu$ g/ml FSC-RGD<sub>3</sub>, or 22.32  $\mu$ g/ml THP-RGD<sub>3</sub>), followed by preparing a dilution scheme for each compound, in which twelve dilutions of every compound (3  $\mu$ M – 5.08×10<sup>-5</sup>  $\mu$ M) were prepared.

The tracer used in this assay was <sup>111</sup>In-labeled DOTA-RGD<sub>2</sub>. <sup>111</sup>In-labeled DOTA-RGD<sub>2</sub> was prepared by adding 29.9  $\mu$ l (0.17 MBq) <sup>111</sup>InCl<sub>3</sub> solution to 1  $\mu$ l peptide dissolved in 60  $\mu$ l 0.5M MES buffer (2-(N-morpholino)ethanesulfonic acid), pH5.5. After 20 minutes at 95°C, <sup>111</sup>In-labeled DOTA-RGD<sub>2</sub> was further purified using an Oasis<sup>®</sup> HLB (1 cm<sup>3</sup>, 30 mg) cartridge (Waters, Milford, MA, USA). The tracer was purified on the HLB cartridge: the labeling reaction mixture was subsequently washed with 3 × 1 ml H<sub>2</sub>O. The <sup>111</sup>In-labeled DOTA-RGD<sub>2</sub> was eluted from the cartridge with 200  $\mu$ l 100% EtOH in H<sub>2</sub>O (v/v).

The radiochemical purity of <sup>111</sup>In-labeled DOTA-RGD<sub>2</sub> was determined using instant thin-layer chromatography (ITLC) using TECControl<sup>™</sup> chromatography strips (Biodex Medical Systems, Shirley, NY, USA). The mobile phases used was 0.1M CH<sub>3</sub>COONH<sub>4</sub>/0.1 M EDTA (1:1 v/v). The strip was analyzed using a Fujifilm BAS-1800II Scanner (Fuji Photo Film Co., Tokyo, Japan).

Two microtiter 96-well vinyl assay plates (Corning B.V., Schiphol-Rijk, The Netherlands) were coated with 100  $\mu$ l/well of a solution of purified human  $\alpha_v\beta_3$  integrin (150 ng/ml) (Chemicon International, Temecula, CA, USA) in coating buffer for 16 hours at 4°C. The plates were then washed twice with 150  $\mu$ l/well binding buffer and filled with 200  $\mu$ l/well blocking buffer. After 2 hours at room temperature, the plates were washed twice with 150  $\mu$ l/well binding buffer. 50  $\mu$ l/well of the appropriate dilution was added to each well, directly followed by 50  $\mu$ l/well <sup>111</sup>In-labeled DOTA-RGD<sub>2</sub>. The solution incubated at 37°C for 1 hour. After incubation, the wells were washed for 3 times with binding buffer (150  $\mu$ l/well).

The wells were cut out and the amount of radioactivity was counted in the gamma counter, together with 1% standards. The experiment was performed in triplicate.

A non-linear regression data fit was performed after plotting the results on a semi-logarithmic scale (log of binding concentration on x-axis and response linear on y-axis). The values were normalized for the dimeric compound (DOTA-RGD<sub>2</sub>) as 100%. The half-maximal inhibitory concentration (IC<sub>50</sub>) values were calculated as mean  $\pm$  standard deviation using non-linear regression model in Graphpad Prism version 5.03.

#### Tumor, animal and cell culture model

Thirty-two 6- to 8-wk-old female BALB/c Nude mice (BALB/c nu/nu/Foxn1nu, Janvier) with subcutaneously xenografted SK-RC-52 renal cell carcinomas were used. The SK-RC-52 cells were cultured and maintained in RPMI medium supplemented with glutamine and fetal calf serum (RPMI++), at 37°C in a humidified atmosphere with 5% CO<sub>2</sub>. The mice acclimatized for 7 days after transportation to the animal facility. The animals (4 mice/cage) were housed in filter-topped cages in a specific pathogen-free unit in accordance with institutional guidelines. Subsequently, the mice were injected subcutaneously (s.c.) in the left flank with a concentration of 2×10<sup>6</sup> SK-RC-52 cells in 200 mL of RPMI++ medium per mouse. Tumors were allowed to grow for 2 weeks until they reached a diameter of approximately 6 mm. The Animal Welfare Committee of the Radboud University Nijmegen Medical Centre approved the animal experiments.

#### Biodistribution study

Twenty mice were injected via tail vein with one of the four <sup>68</sup>Ga-labeled RGD peptides. Each injection contained 0.5 nmol and approximately 10 MBq <sup>68</sup>Ga-labeled peptide in a volume of 300  $\mu$ l per mouse. All mice were euthanized by CO<sub>2</sub>/O<sub>2</sub> asphyxiation 60 minutes post injection. Tissue samples (tumor, blood, heart, lung, liver, stomach, kidney, spleen, pancreas, duodenum, muscle, bladder, and adrenal glands) were dissected. The weights of all tissue samples were measured and their activity was determined with a gamma counter simultaneously with 1% standards of the injected dose.

The biodistribution data are expressed as mean percentage injected dose per gram (%ID/g)  $\pm$  standard deviation. Statistical analysis was performed using one-way ANOVA assuming Gaussian distribution. Multiple comparison after one-way ANOVA by means of a two tailed t-test was applied using GraphPad Prism version 5.03. A p-value of <0.05 was considered as statistically significant difference between the radiotracers.

#### $\alpha_v\beta_3$ integrin specificity (blocking experiment)

The specificity of the RGD binding of each compound was investigated in a blocking experiment. Twelve mice were injected via tail vein with <sup>68</sup>Ga-labeled RGD peptide (0.5 nmol, 10 MBq) and an excess unlabeled DOTA-RGD<sub>2</sub> (50 nmol). The biodistribution data are expressed as mean percentage injected dose per gram (%ID/g)  $\pm$  standard deviation.

#### PET imaging

For each tracer three mice were scanned using a small-animal PET/CT scanner (Inveon<sup>®</sup>, Siemens Medical Solutions, Knoxville, TN, USA). The mice were placed with head first in a prone position in the scanner. The PET images were acquired for 20, 30, or 40 minutes, with an intrinsic spatial resolution

of 1.5 mm. A CT scan was performed for anatomical localization and was acquired after PET imaging, with a spatial resolution of 113  $\mu\text{m}$ , 80 kV, 500  $\mu\text{A}$ , and exposure time of 300 ms. Immediately after scanning, tissues samples of these mice were collected as described above.

PET data were reconstructed using Inveon Acquisition Workplace software version 2.04 (Siemens Preclinical Solutions, Knoxville, TN, USA), using Maximum a Posteriori (MAP) algorithm (form of Ordered Subset Expectation Maximisation 3-D (OSEM3D)) with a matrix of  $256 \times 256 \times 161$ , pixel size of  $0.40 \times 0.40 \times 0.796 \text{ mm}^3$ , 16 OSEM3D subsets and 2 iterations. Post reconstruction filtering was performed using 3D Gaussian filter kernel with full width half maximum (FWHM) of 1.5 mm.

CT data were reconstructed using a modified Feldkamp algorithm at the INVEON CT Recon Software, Version 2.04 (Siemens Preclinical Solutions, Knoxville, TN, USA). The resulting matrix was  $768 \times 786$  pixels with 512 transverse slices (voxel size of  $110.5 \times 110.5 \times 110.5 \mu\text{m}^3$ ). The  $^{68}\text{Ga}$ -PET and CT images were fused for anatomical reference using automatic rigid registration software available at the workstation. The registration was visually checked. The biodistribution pattern was visualized using the Inveon Research Workplace (Siemens, Knoxville, TN, USA).

## Results

### Radiolabeling

A radiochemical purity of >95% was obtained for all labeling procedures. The ITLC profiles demonstrated a purity ranging from 96.7 – 99.9% and for the ITLC-colloid profiles, the purities ranged from 74.0 – 100%. RP-HPLC analysis indicated that the purities were >90%, showing single peaks for each labeling of each compound. Retention times ranged from 14.5 to 14.9 minutes.

### Solid-phase $\alpha_v\beta_3$ integrin binding assay

The affinity of the four tracers for  $\alpha_v\beta_3$  integrin was determined in a competitive binding assay. The binding  $^{111}\text{In}$ -labeled DOTA-RGD<sub>2</sub> was competed by all four unlabeled radiotracers in a concentration dependent manner. The binding affinity of DOTA-RGD<sub>2</sub> ( $\text{IC}_{50} = 3.79 \pm 0.65 \text{ nM}$ ) was significantly different from the of TRAP-RGD<sub>3</sub> ( $\text{IC}_{50} = 10.0 \pm 1.81 \text{ nM}$ ,  $p = 0.005$ ), FSC-RGD<sub>3</sub>, ( $\text{IC}_{50} = 9.02 \pm 1.61 \text{ nM}$ ,  $p=0.006$ ), and THP-RGD<sub>3</sub> ( $\text{IC}_{50} = 11.38 \pm 1.88 \text{ nM}$ ,  $p=0.003$ ). The results of the  $\alpha_v\beta_3$  integrin binding assay are depicted in Figure 6.

### Biodistribution

Twenty mice were injected via tail vein. The mean administered activity for the mice were 13.96 MBq (12.9-14.8) for  $^{68}\text{Ga}$ -DOTA-RGD<sub>2</sub>, 11.17 MBq (11.10-11.25) for  $^{68}\text{Ga}$ -TRAP-RGD<sub>3</sub>, 13.2 MBq (12.7-13.66) for  $^{68}\text{Ga}$ -FSC-RGD<sub>3</sub>, and 13.4 MBq (12.5-13.79) for  $^{68}\text{Ga}$ -THP-RGD<sub>3</sub>.

The mean administered activity for the twelve mice with excess cold were 5.1 MBq (4.8-5.2) for  $^{68}\text{Ga}$ -DOTA-RGD<sub>2</sub>, 11.8 MBq (11.4-12.1) for  $^{68}\text{Ga}$ -TRAP-RGD<sub>3</sub>, 11.6 MBq (11.3-11.8) for  $^{68}\text{Ga}$ -FSC-RGD<sub>3</sub>, and 11.9 MBq (11.6-12.2) for  $^{68}\text{Ga}$ -THP-RGD<sub>3</sub>.

The results of the biodistribution study of the  $^{68}\text{Ga}$ -labeled peptides,  $^{68}\text{Ga}$ -DOTA-RGD<sub>2</sub>,  $^{68}\text{Ga}$ -TRAP-RGD<sub>3</sub>,  $^{68}\text{Ga}$ -FSC-RGD<sub>3</sub>, and  $^{68}\text{Ga}$ -THP-RGD<sub>3</sub> respectively, are depicted in Figure 7. Tumor uptake values were  $5.1 \pm 2.7 \text{ \%ID/g}$ ,  $4.3 \pm 0.8 \text{ \%ID/g}$ ,  $8.5 \pm 1.4 \text{ \%ID/g}$ , and  $5.3 \pm 0.6 \text{ \%ID/g}$ , for  $^{68}\text{Ga}$ -labeled DOTA-RGD<sub>2</sub>, TRAP-RGD<sub>3</sub>, FSC-RGD<sub>3</sub>, and THP-RGD<sub>3</sub> respectively. There were significant differences in tumor uptake

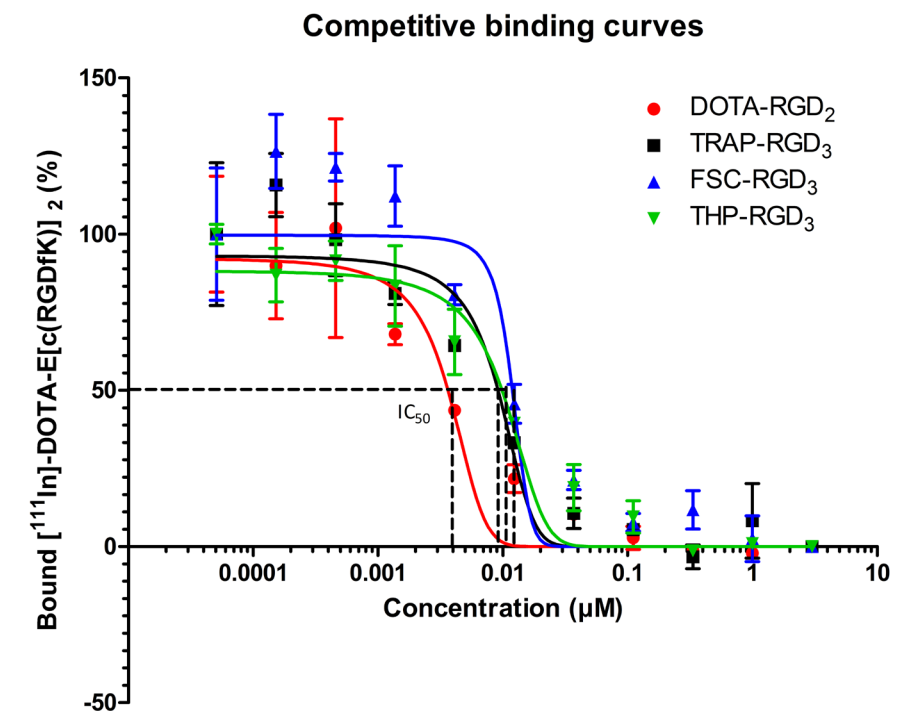


**Figure 6.** Competitive binding curves on semi-logarithmic scale of  $^{111}\text{In}$ -labeled DOTA-RGD<sub>2</sub> on  $\alpha_v\beta_3$  integrin with added unlabeled DOTA-RGD<sub>2</sub>, TRAP-RGD<sub>3</sub>, FSC-RGD<sub>3</sub>. Expressed as percentage of DOTA-RGD<sub>2</sub> binding.

between  $^{68}\text{Ga}$ -DOTA-RGD<sub>2</sub> and  $^{68}\text{Ga}$ -FSC-RGD<sub>3</sub> ( $p=0.0285$ ), between the  $^{68}\text{Ga}$ -TRAP-RGD<sub>3</sub> and  $^{68}\text{Ga}$ -FSC-RGD<sub>3</sub> ( $p=0.0004$ ), and between  $^{68}\text{Ga}$ -FSC-RGD<sub>3</sub> and  $^{68}\text{Ga}$ -THP-RGD<sub>3</sub> ( $p=0.0018$ ).

All four tracers rapidly cleared from the blood, except for  $^{68}\text{Ga}$ -FSC-RGD<sub>3</sub>, showing  $2.37 \pm 0.13 \text{ \%ID/g}$  present within the blood after one hour. Blood uptake values were statistically significantly different from each other, each showing  $p$ -values of  $p<0.0001$ , except for  $^{68}\text{Ga}$ -DOTA-RGD<sub>2</sub> and  $^{68}\text{Ga}$ -TRAP-RGD<sub>3</sub> where  $p=0.0065$ . Uptake values of the blood were  $0.20 \pm 0.05 \text{ \%ID/g}$ ,  $0.11 \pm 0.02 \text{ \%ID/g}$ ,  $2.37 \pm 0.13 \text{ \%ID/g}$ , and  $0.40 \pm 0.03 \text{ \%ID/g}$ , for  $^{68}\text{Ga}$ -DOTA-RGD<sub>2</sub>,  $^{68}\text{Ga}$ -TRAP-RGD<sub>3</sub>,  $^{68}\text{Ga}$ -FSC-RGD<sub>3</sub>, and  $^{68}\text{Ga}$ -THP-RGD<sub>3</sub> respectively.

The uptake values within the muscle were  $0.33 \pm 0.10 \text{ \%ID/g}$ ,  $0.21 \pm 0.01 \text{ \%ID/g}$ ,  $0.71 \pm 0.02 \text{ \%ID/g}$ , and  $0.47 \pm 0.02 \text{ \%ID/g}$  for  $^{68}\text{Ga}$ -DOTA-RGD<sub>2</sub>,  $^{68}\text{Ga}$ -TRAP-RGD<sub>3</sub>,  $^{68}\text{Ga}$ -FSC-RGD<sub>3</sub>, and  $^{68}\text{Ga}$ -THP-RGD<sub>3</sub> respectively.

The uptake of  $^{68}\text{Ga}$ -DOTA-RGD<sub>2</sub> in the kidneys ( $2.67 \pm 0.27 \text{ \%ID/g}$ ) was statistically significantly lower compared to the uptake of  $^{68}\text{Ga}$ -TRAP-RGD<sub>3</sub> ( $4.00 \pm 0.44 \text{ \%ID/g}$ ,  $p=0.0004$ ),  $^{68}\text{Ga}$ -FSC-RGD<sub>3</sub> ( $15.65 \pm 0.86$ ,  $p<0.0001$ ), and  $^{68}\text{Ga}$ -THP-RGD<sub>3</sub> ( $8.88 \pm 0.81 \text{ \%ID/g}$ ,  $p<0.0001$ ). The other compounds also differed significantly from each other (data is not shown).

Tumor-to-blood (TBR), tumor-to-muscle ratios (TMR), and tumor-to-kidney ratios (TKR) with standard deviations were calculated and are summarized in Table 3. The lowest TBR was found for  $^{68}\text{Ga}$ -FSC-RGD<sub>3</sub>, mainly due to the higher blood values. The TBR between  $^{68}\text{Ga}$ -FSC-RGD<sub>3</sub> and the other compounds were significant different ( $^{68}\text{Ga}$ -DOTA-RGD<sub>2</sub>,  $p=0.0131$ ,  $^{68}\text{Ga}$ -TRAP-RGD<sub>3</sub>,  $p=0.005$ , and  $^{68}\text{Ga}$ -THP-RGD<sub>3</sub>,  $p<0.0001$ ).

Table 3. Tumor-to-Blood Ratio (TBR), Tumor-to-Muscle Ratio (TMR), and Tumor-to-Kidney Ratio (TKR) calculated from biodistribution data.

	$^{68}\text{Ga-DOTA-RGD}_2$	$^{68}\text{Ga-TRAP-RGD}_3$	$^{68}\text{Ga-FSC-RGD}_3$	$^{68}\text{Ga-THP-RGD}_3$
TBR	17.81 ± 9.39	31.46 ± 15.79	4.24 ± 1.83	13.47 ± 1.54
TMR	14.86 ± 4.26	20.90 ± 3.57	12.03 ± 2.14	11.32 ± 1.72
TKR	1.85 ± 0.87	1.09 ± 0.13	0.55 ± 0.10	0.61 ± 0.11

Figure 8 shows the biodistribution results of tracer and tracer with the addition of excess cold of the dimeric (a) and three trimeric peptides (b-d). A co-injection of unlabeled excess cold of DOTA-RGD<sub>2</sub> resulted in tumor uptake values less than 1.0 %ID/g (0.36 ± 0.01 %ID/g, 0.34 ± 0.07 %ID/g, 0.84 ± 0.03 %ID/g, and 0.64 ± 0.11 %ID/g for the  $^{68}\text{Ga-DOTA-RGD}_2$ , TRAP-RGD<sub>3</sub>, FSC-RGD<sub>3</sub>, and THP-RGD<sub>3</sub> compound respectively). The other dissected organs also showed reduced uptake in the RGD-based radiotracers, suggesting that at least a part of the uptake of the  $^{68}\text{Ga}$ -labeled peptides was  $\alpha_v\beta_3$  integrin mediated. It can be seen that the kidney uptake of all tracers is only partly blocked. This is caused by  $\alpha_v\beta_3$  integrin targeting on the endothelial cells and on the other hand due to renal excretion.

#### PET/CT imaging

PET/CT images were made after CO<sub>2</sub>/O<sub>2</sub> asphyxiation. For all tracers, the PET/CT images showed clearly visible tumors in the left flank. PET/CT images showed high uptake in the abdominal region (intestines and kidneys) for  $^{68}\text{Ga-DOTA-RGD}_2$ ,  $^{68}\text{Ga-FSC-RGD}_3$ , and  $^{68}\text{Ga-THP-RGD}_3$ . The images as shown in Figure 9 are in line with the biodistribution data.

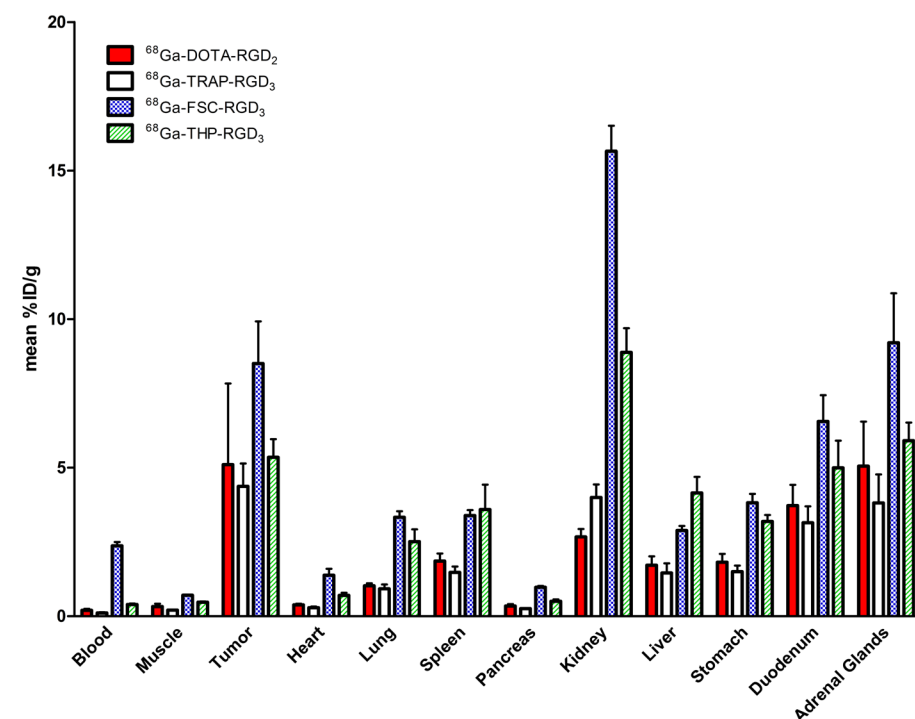


Figure 7. Biodistribution results of the four different  $^{68}\text{Ga}$ -labeled RGD-peptides at 1 hour post-injection. Mice with a SK-RC-52 xenograft tumor in the left flank. The results are expressed as mean percentage of the injected dose per gram (%ID/g) ± standard deviation (0.5 nmol, 5 mice/group).

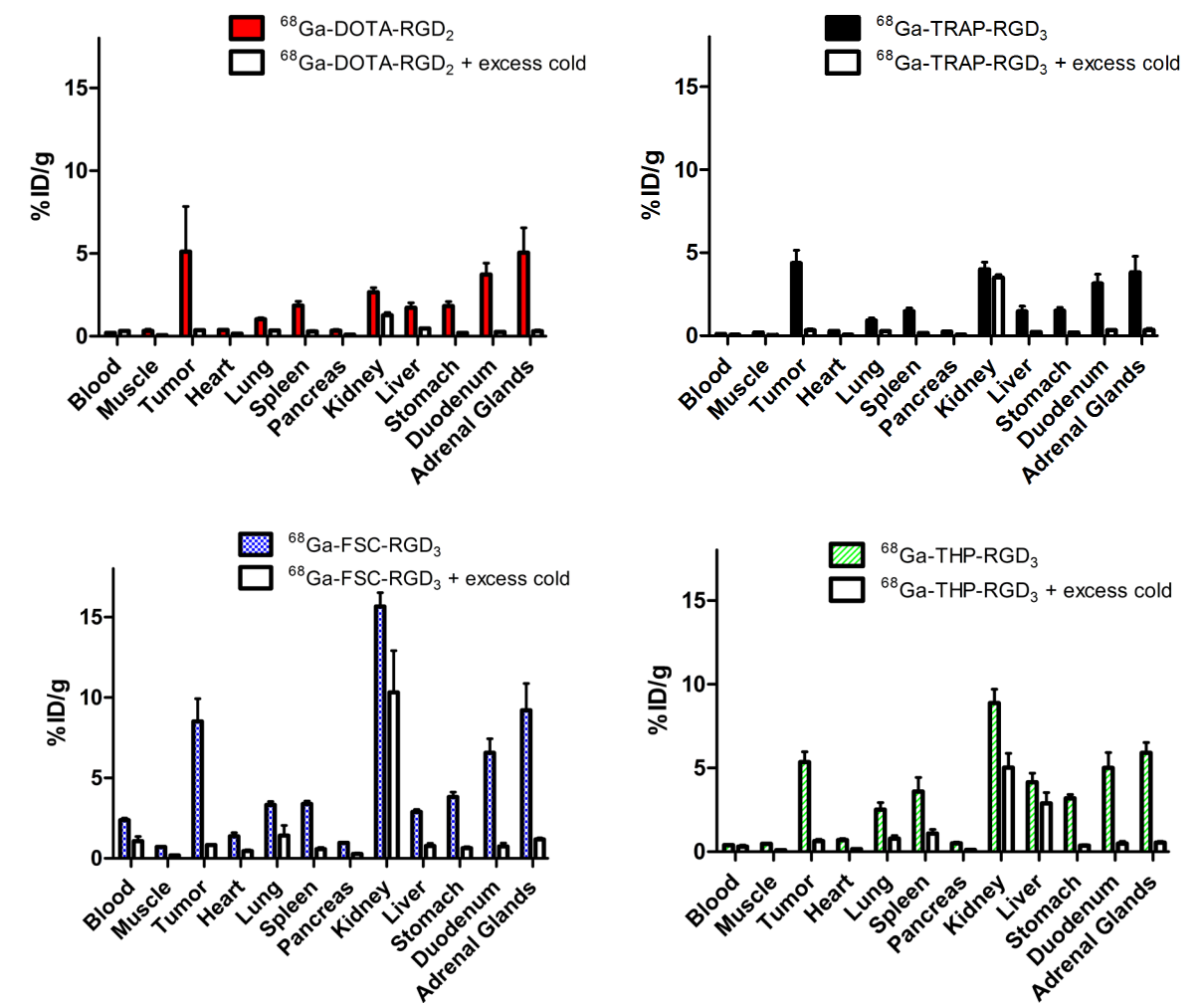


Figure 8. Distribution of radioactivity (black bars) as percentage of injected dose per gram ± standard deviation (%ID/g ± stdev, 5 mice/group), 1 hour post-injection of 0.5 nmol, 11.1-14.8 MBq/mouse with  $^{68}\text{Ga}$ -labeled RGD peptide in SK-RC-52 xenograft tumor model. The blocking dose (white bars) was administered simultaneously with  $^{68}\text{Ga}$ -labeled RGD peptide in SK-RC-52 xenograft tumor model (3 mice/group, 4.8-12.2 MBq/mouse, 0.5 nmol + 50 nmol excess cold of DOTA-RGD<sub>2</sub>), and the results are given as %ID/g ± stdev, 1 hour post-injection.

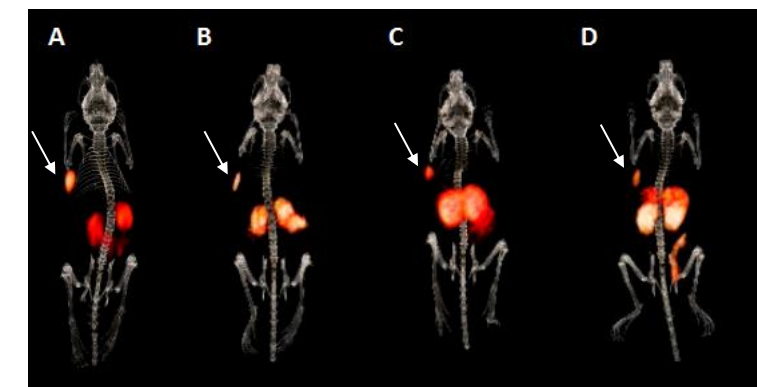


Figure 9. PET/CT 3D image reconstructions of the uptake of an administered peptide dose ranging from 11.1 to 14.8 MBq  $^{68}\text{Ga}$ -DOTA-RGD<sub>2</sub> (A),  $^{68}\text{Ga}$ -TRAP-RGD<sub>3</sub> (B),  $^{68}\text{Ga}$ -FSC-RGD<sub>3</sub> (C), and  $^{68}\text{Ga}$ -THP-RGD<sub>3</sub> (D), 1 hour after injection. Scaling was performed for each mouse separately, to show a clearly visible tumor in each case (optimal scaling). White arrows indicate tracer uptake in tumor tissue.

### Discussion

In this study four multimeric cyclic RGD-based radiotracers were selected: <sup>68</sup>Ga-DOTA-RGD<sub>2</sub>, <sup>68</sup>Ga-TRAP-RGD<sub>3</sub>, <sup>68</sup>Ga-FSC-RGD<sub>3</sub>, and <sup>68</sup>Ga-THP-RGD<sub>3</sub>, to study the *in vitro* and *in vivo*  $\alpha_v\beta_3$  integrin targeting characteristics of each tracer within a single experiment. These radiopharmaceuticals were developed to improve the binding affinity for  $\alpha_v\beta_3$  integrin. <sup>68</sup>Ga-DOTA-RGD<sub>2</sub> showed optimal *in vivo*  $\alpha_v\beta_3$  integrin targeting properties with slightly better affinity for  $\alpha_v\beta_3$  integrin compared to <sup>68</sup>Ga-TRAP-RGD<sub>3</sub>, <sup>68</sup>Ga-FSC-RGD<sub>3</sub> and <sup>68</sup>Ga-THP-RGD<sub>3</sub>. However, all four radiotracers showed receptor specific imaging of  $\alpha_v\beta_3$  integrin expression and also showed sufficient tumor targeting.

During the labeling procedure of the RGD-based peptides, formation of <sup>68</sup>Ga-colloid may occur. In case of <sup>68</sup>Ga-colloid formation, enhanced accumulation of this <sup>68</sup>Ga-colloid within the liver and spleen will be observed. Tracer uptake in abdominal tumor tissue may interfere with this enhanced accumulation, consequently resulting in reduced image quality. The ITLC-colloid method is used to test this phenomenon and in case of the formation of colloid, the labeled peptide is purified with an HLB cartridge. During the radiolabeling procedure of <sup>68</sup>Ga-THP-RGD<sub>3</sub>, 26% of <sup>68</sup>Ga-colloid was observed, suggesting that <sup>68</sup>Ga-colloid was present. However, tracer uptake within the liver and spleen did not differ from the other compounds, making it less likely <sup>68</sup>Ga-colloid was indeed present. Accurate analysis is only possible when the ITLC-colloid method has been optimized. In case of <sup>68</sup>Ga-THP-RGD<sub>3</sub>, it is suggested to determine the correct buffer solution in order to optimize the ITLC-colloid method.

Several groups tried to increase the binding affinity and tried to enhance the tumor targeting properties. In this study, the binding of <sup>111</sup>In-DOTA-RGD<sub>2</sub> to  $\alpha_v\beta_3$  integrin competed by unlabeled DOTA-RGD<sub>2</sub>, TRAP-RGD<sub>3</sub>, FSC-RGD<sub>3</sub>, and THP-RGD<sub>3</sub> compound, was determined in the solid phase binding assay. We showed that the dimeric compound has binding affinities in the same nM range as the trimeric counterparts, if tested under equal circumstances and using equimolar peptide doses. The small variation in binding affinities between the radiotracers may be attributed to the influence of the different chemical structures. When the results are compared with the binding affinities as mentioned in literature, our results seem to be comparable (in the same nM range). However, this comparison and the interpretation should be done carefully, since different experimental set-ups were used to determine the IC<sub>50</sub> values [49, 59-61]. Another limitation that should be considered when interpreting the results is that the detection of the emitted gamma rays were near the detection rate of the gamma-counter and furthermore binding to  $\alpha_v\beta_3$  integrin was low, suggesting a suboptimal binding assay. Therefore, a new binding assay might be considered.

<sup>68</sup>Ga-FSC-RGD<sub>3</sub> showed a remarkable difference in kidney, blood, and tumor uptake. The TBR and TKR were significantly lower than that of the other three radiotracers (<sup>68</sup>Ga-DOTA-RGD<sub>2</sub>, <sup>68</sup>Ga-TRAP-RGD<sub>3</sub>, and <sup>68</sup>Ga-THP-RGD<sub>3</sub>). The differences in TBRs are probably attributed to the much slower blood clearance, that was also seen in the study conducted by Zhai *et al.* (TMR were 6.4 ± 2.5 (1 hour p.i. and 18.7 ± 2.7 2 hours p.i.) [59]. They stated that the differences in blood clearance compared to <sup>68</sup>Ga-TRAP-RGD<sub>3</sub> could be related to the different charge of the FSC chelator or by the longer blood circulation due to free Gallium-68 bound to transferrin. Therefore, the <sup>68</sup>Ga-FSC-RGD<sub>3</sub> peptide is a less attractive choice for imaging  $\alpha_v\beta_3$  integrin in clinical practice.

The uptake in non-tumor tissue are relatively low, as observed by the biodistribution data of the  $\alpha_v\beta_3$  integrin positive SK-RC-52 tumors at 1 hour post injection for all tracers. In the experiment with the

excess unlabeled RGD peptide, the uptake in non-tumor tissue was further decreased, suggesting that the uptake of the RGD-based radiotracers in these organs is at least partially  $\alpha_v\beta_3$  integrin mediated. This conclusion can be supported by the immunohistochemistry study of Wu *et al.*, in which the liver, lung, and kidney tissue were positive for the anti  $\beta_3$ -antibody [63]. The uptake of <sup>68</sup>Ga-FSC-RGD<sub>3</sub> and <sup>68</sup>Ga-THP-RGD<sub>3</sub> in non-tumor tissue, e.g. blood, kidney, heart, stomach, duodenum, adrenal glands, spleen, liver, and lungs are significantly higher than the uptake of <sup>68</sup>Ga-DOTA-RGD<sub>2</sub> and <sup>68</sup>Ga-TRAP-RGD<sub>3</sub>. The uptake in non-tumor tissue should be low to be able to detect lesions in areas close to these organs and to prevent unnecessary radiation burden to these tissues. It is therefore suggested to choose <sup>68</sup>Ga-DOTA-RGD<sub>2</sub> or <sup>68</sup>Ga-TRAP-RGD<sub>3</sub> for further *in vivo* studies instead of <sup>68</sup>Ga-FSC-RGD<sub>3</sub> and <sup>68</sup>Ga-THP-RGD<sub>3</sub>.

The tracer accumulation in the adrenal glands was investigated because the biodistribution data obtained by Notni *et al.* [60], showed an extremely high uptake in the adrenal gland (27.77 ± 9.97 %ID/g) which seems to be specific, since the blocking experiment showed low tracer uptake (0.36 ± 0.05 %ID/g). Gladson *et al.* stated that  $\alpha_v\beta_3$  integrin could be a useful marker of undifferentiated neuroblastoma cells present in adrenal glands, since a decrease in expression was observed when undifferentiated neuroblastoma cells differentiated into mature ganglion or neuronal cells [64]. This suggests that there is at least partly  $\alpha_v\beta_3$  integrin expression present within the adrenal glands. The authors did not have an explanation for the high uptake values. Compared with the biodistribution data of this study, the mean tracer uptake in the adrenal glands was much lower (< 10 %ID/g for all four compounds). Perhaps the difference in tracer uptake is the effect of a different peptide dose used in the *in vivo* experiment.

Because multimeric peptides showed enhanced receptor affinity compared to monomeric analogs in previous studies [48, 55, 56, 63, 65], it was thought that the dimeric radiolabeled peptide <sup>68</sup>Ga-DOTA-RGD<sub>2</sub> would not be the best option as radiotracer for  $\alpha_v\beta_3$  integrin imaging in clinical practice compared to the trimeric RGD-based peptides. For this experiment, equimolar amounts of each radiolabeled RGD-based peptide were used. Because of the differences in numbers of RGD units within a molecule, trimeric RGD-based peptides provide 1.5 times as much active binding sites as an equimolar amount of the dimeric RGD-based peptide. However, based on the results obtained in this study, multimerization is not the only factor influencing the receptor binding affinity. The choice of linkers used in multimeric RGD-based peptides could also influence the possibility to bind  $\alpha_v\beta_3$  integrins [66]. The chemical structure may affect 'statistical rebinding', a term that was introduced by Dijkgraaf *et al.* [49]. Statistical rebinding means that the number of RGD peptides present within one molecule can affect the chance of (re)binding the receptor, and in this way enhance receptor targeting. On the other hand, the chemical structure may prevent rebinding. The chemical structures of the radiolabeled peptides used in this study are different and therefore may explain the differences in binding affinities of <sup>68</sup>Ga-DOTA-RGD<sub>2</sub> and the trimeric peptides <sup>68</sup>Ga-TRAP-RGD<sub>3</sub>, <sup>68</sup>Ga-FSC-RGD<sub>3</sub>, and <sup>68</sup>Ga-THP-RGD<sub>3</sub>.

### Conclusion

<sup>68</sup>Ga-DOTA-RGD<sub>2</sub> and <sup>68</sup>Ga-TRAP-RGD<sub>3</sub> showed optimal *in vivo*  $\alpha_v\beta_3$  integrin targeting properties compared to <sup>68</sup>Ga-FSC-RGD<sub>3</sub> and <sup>68</sup>Ga-THP-RGD<sub>3</sub>, due to higher TBR and TMR ratios and lower tracer uptake in non-tumor tissue (e.g. kidneys), making them more suitable radiotracers for PET/CT imaging to image  $\alpha_v\beta_3$  integrin expression. Because of the extensive (clinical) experience using DOTA-conjugated radiopharmaceuticals and because of the available equipment present at our department, <sup>68</sup>Ga-DOTA-RGD<sub>2</sub> will be chosen for further clinical studies.

## Chapter 3: Imaging of angiogenesis in HNSCC patients using <sup>68</sup>Ga-DOTA-RGD<sub>2</sub> PET/CT

### Introduction

Angiogenesis is a crucial process for tumor growth and metastasis. Non-invasive methods to monitor angiogenesis in tumor lesions could be of great value for treatment selection and adaptation, or for response monitoring to steer patient management aiming to improve patient outcome as well as to enhance patients' quality of life. Especially in patients with HNSCC, quality of life is an important factor to consider. Treatment induces significant morbidity which include swallowing and speech impairment, loss of shoulder function, mucositis, dermatitis, dysphagia, a dry mouth or thickened saliva, or fatigue. Optimal treatment while preserving the function of the organs in the head and neck region needs thorough investigation of all available treatment options.

Several imaging biomarkers depict fundamental processes involved in tumor biology. Research on the process of angiogenesis resulted in the identification of several biomarkers, that could be used to develop tracers for radionuclide imaging of angiogenesis. One of the promising targeted agents for PET/CT is <sup>68</sup>Ga-DOTA-RGD<sub>2</sub>. During angiogenesis,  $\alpha_v\beta_3$  integrins are expressed on newly formed endothelial cells. <sup>68</sup>Ga-DOTA-RGD<sub>2</sub> targeting agent mimics the binding potential of proteins of the extracellular matrix (fibronectin, vitronectin, laminin, a.o.) by targeting  $\alpha_v\beta_3$  integrin expression via their RGD sequence.

The studies in mice with human tumor xenografts showed the feasibility of imaging angiogenesis using <sup>68</sup>Ga-DOTA-RGD<sub>2</sub> in HNSCC [49-51]. Furthermore, immunohistochemical staining profiles of the tumor tissue confirmed the sole expression of  $\alpha_v\beta_3$  integrin on neovascular structures within the tumor and not on tumor cells themselves [50]. The data acquired in these preclinical experiments provided clear evidence that <sup>68</sup>Ga-labeled DOTA-RGD<sub>2</sub> can be used as an imaging biomarker of angiogenesis and that it could be an useful tool to monitor therapy responses. The aim of the current study is to test this new radiotracer for PET/CT imaging of  $\alpha_v\beta_3$  integrin expression in patients with HNSCC. When successful, this non-invasive imaging method may be of great value for selection and adaptation of treatment, or as response monitoring tool to steer treatment decisions early after start of treatment.

### Study objectives

This will be the first clinical imaging study using <sup>68</sup>Ga-DOTA-RGD<sub>2</sub> PET/CT to image  $\alpha_v\beta_3$  integrin expression in HNSCC. The primary objectives of this study are to assess the feasibility and safety of <sup>68</sup>Ga-DOTA-RGD<sub>2</sub> PET/CT imaging in patients. Secondary objectives are to determine the biodistribution, pharmacokinetics, and pharmacodynamics of <sup>68</sup>Ga-DOTA-RGD<sub>2</sub>. Furthermore, we aim to validate <sup>68</sup>Ga-DOTA-RGD<sub>2</sub> as an imaging biomarker of angiogenesis, using immunohistochemical analysis: the correlation between <sup>68</sup>Ga-DOTA-RGD<sub>2</sub> uptake in tumor lesions and the expression of  $\alpha_v\beta_3$  integrin on the tumor vasculature is determined.

### Outcome measures

The primary outcome measures are the quantitative analysis of <sup>68</sup>Ga-DOTA-RGD<sub>2</sub> tracer uptake in tumor tissue, using Standardized Uptake Values (SUV), and the recording of adverse events, changes in vital signs, and laboratory measurements before, during, and after radiotracer injection. Secondary outcome measures include the quantitative analysis of tracer uptake in other organs, such as the liver, kidneys, muscle, a.o. Secondary outcome measures further include the pharmacodynamic analysis of <sup>68</sup>Ga-DOTA-

RGD<sub>2</sub> by deducing the arterial plasma time–activity concentration curve (APTAC) and the tissue time–activity curve (TTAC) from dynamic PET data. With the pharmacokinetic and pharmacodynamic imaging data the optimal scan time will be determined. The optimal time point for tumor imaging is defined as the time with the highest uptake in tumor tissue and the lowest uptake in non-tumor tissue, resulting in the highest tumor-to-background ratio (TBR). The last secondary outcome measure is the semi-quantitative analysis of the  $\alpha_v\beta_3$  integrin expression on the tumor vasculature. The tracer uptake (SUV) as determined with PET/CT will be correlated with the expression of  $\alpha_v\beta_3$  integrin as determined with immunohistology.

### Study design

#### Study population

The study protocol, written as part of this thesis, was reviewed by the institutional Committee on Ethics (see appendix A). Patients presenting in the Radboud University Medical Center are considered for recruitment, if they are over the age of 18 years and able to provide written informed consent. We prospectively include patients who are scheduled to undergo surgical resection of a proven squamous cell carcinoma of the oral cavity, oro- and hypopharynx, or larynx.

The study population for this pilot study exists of 25 evaluable patients. Patients are included consecutively. In order to be eligible to participate in this study, a subject meet all of the following criteria.

#### Inclusion criteria

All patients have at least one proven tumor lesion of the oral cavity, oro- and hypopharynx, or larynx, with a diameter of at least 3 cm. The diameter is examined during the clinical examination and according to radiologic criteria obtained from either MRI or CT. A diagnostic CT or MRI scan is obtained within four weeks prior to the screening visit. A surgery as primary treatment should be planned.

The patient should not have any of the following contra-indications for PET/CT; pregnancy, breast-feeding, or severe claustrophobia, nor an impaired renal function (Creatinin clearance  $\leq$  60 mL/min according to the ‘The Cockcroft-Gault’ equation), or an impaired liver function (ALAT, ASAT  $\geq$  3x ULN, and total bilirubin  $\geq$  2x ULN). Patients are excluded if they are diagnosed with other serious illnesses.

#### Safety analysis

In ten patients, safety of <sup>68</sup>Ga-DOTA-RGD<sub>2</sub> administration will be evaluated. Safety monitoring includes the recording of adverse events, changes in vital signs, and laboratory measurements before, during and after the injection of <sup>68</sup>Ga-DOTA-RGD<sub>2</sub>. Vital signs are evaluated at baseline and 120 minutes after injection and include blood pressure, temperature, and heart rate. Changes in liver and kidney function (alanine aminotransferase (ALAT), aspartate aminotransferase (ASAT), creatinine clearance, bilirubin, and ureum) are studied and therefore two blood samples are obtained. One blood sample is drawn before injection of the radioactive tracer (baseline measurement), the second venous puncture is performed 24 hours after administration of <sup>68</sup>Ga-DOTA-RGD<sub>2</sub>. Hematology lab values (Hb, Ht, leucocytes, and thrombocytes) are also determined at both time points.

During examination, blood samples of 3 mL are drawn for pharmacokinetic analysis at 5, 30, 60, 90, and 120 minutes after administration of <sup>68</sup>Ga-DOTA-RGD<sub>2</sub>. All measurements are written down in the subject’s source records. Patients are monitored further if abnormalities in laboratory measurements are detected.

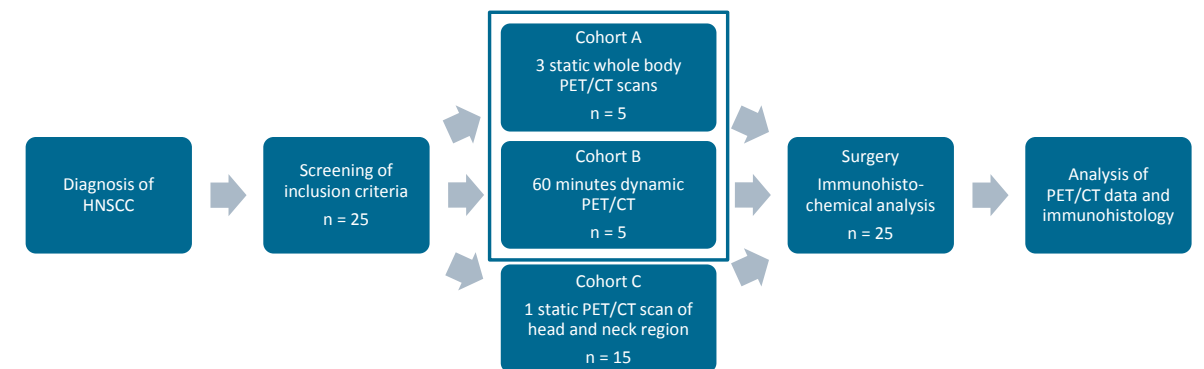


**Figure 10.** Flowchart of study design. Blue box indicates the ten patients in which safety of <sup>68</sup>Ga-DOTA-RGD<sub>2</sub> administration is evaluated.

#### PET/CT scan protocol

To determine the feasibility of <sup>68</sup>Ga-DOTA-RGD<sub>2</sub> PET/CT imaging, and to determine the whole-body distribution, pharmacokinetics, and pharmacodynamics of <sup>68</sup>Ga-DOTA-RGD<sub>2</sub> injection, three scan protocols are applied in three patient cohorts. These are briefly described in the next sections. All patients are scheduled for a <sup>68</sup>Ga-DOTA-RGD<sub>2</sub> PET/CT scan one to seven days before the planned surgery.

#### Study cohort A

In the first five patients three static whole-body PET/CT scans are acquired after <sup>68</sup>Ga-DOTA-RGD<sub>2</sub> injection to assess safety of administration and to determine the biodistribution (e.g. uptake in tumor tissue, stomach, lungs, heart, blood, kidneys, bladder, liver, spleen, muscle, adrenal glands, thyroid tissue, brain, brain ventricles, small and large intestines). From these first five patients, three static whole-body scans of approximately 20 minutes will be acquired, starting 30 minutes after injection of <sup>68</sup>Ga-DOTA-RGD<sub>2</sub>, followed by a scan at 60 minutes, and 90 minutes, respectively.

#### Study cohort B

With a dynamic PET/CT scan protocol, the pharmacokinetics and tumor dynamics is further assessed. Five patients undergo a 60 minutes dynamic PET/CT scan of the head- and neck region. They are positioned within the scanner and the PET/CT scan start immediately after a bolus-injection of <sup>68</sup>Ga-DOTA-RGD<sub>2</sub>.

#### Study cohort C

In the third cohort of 15 patients, the feasibility, safety, and tumor imaging characteristics of the tracer is further evaluated. Therefore, a <sup>68</sup>Ga-DOTA-RGD<sub>2</sub> PET/CT scan of the head and neck region is acquired at the optimal imaging time point several minutes after injection of <sup>68</sup>Ga-DOTA-RGD<sub>2</sub>.

#### Immunohistochemistry

Tumor tissue samples are collected directly after tumor removal. Ideally, a section through the center of the tumor (through cut) is obtained, together with eight samples/biopsies at four poles of the tumor. Multiple samples at both the peripheral side and central part of the tumor and in each quadrant are obtained, when a section through the tumor is not feasible. Formalin-fixed and paraffin-embedded tissue specimens (FFPE) and frozen tumor tissue samples are taken. The FFPE obtained samples are processed in the standard fashion with hematoxylin and eosin (HE) for grading and staging. These

samples are also prepared to perform immunohistochemical analysis of angiogenic specific markers. Microvessel density is determined using anti-human CD34 antibody. The  $\alpha_v\beta_3$  integrin expression is determined on the frozen sections using a specific  $\alpha_v\beta_3$  integrin marker, a biotinylated monoclonal anti- $\alpha_v\beta_3$  antibody, LM609 (1:800; Merck Millipore). Immunohistochemistry staining is visually quantified by an experienced pathologist and is scored based on staining intensity, using a semi-quantitative four-point scale (0 = no staining, 1 = weak, 2 = moderate, and 3 = strong positive staining).

### Materials and method

#### Preparation and injection of <sup>68</sup>Ga-DOTA-RGD<sub>2</sub>

<sup>68</sup>Ga-DOTA-RGD<sub>2</sub> is produced according to GMP-compliant procedures, at the laboratory of the department of Radiology and Nuclear Medicine (Radboudumc, Nijmegen). The <sup>68</sup>Ga-DOTA-RGD<sub>2</sub> radiolabeling procedure is described in detail in the supplementary data of Appendix B. The patients receive 70  $\mu$ g, 200 MBq <sup>68</sup>Ga-DOTA-RGD<sub>2</sub>. No specific subject preparations are requested, e.g. patients are able to take their regular medicines according to their normal schedule, and no fasting or hydration is needed. The <sup>68</sup>Ga-DOTA-RGD<sub>2</sub> is injected as a bolus over one minute. After administration, the syringe is measured for residual activity in order to correct for the administered activity.

#### PET/CT imaging protocol

Patients are scanned with a Biograph 40 mCT PET/CT scanner (Siemens Healthcare). PET and CT images are acquired according to the scan protocol, which depends on the subjects' cohort. The PET/CT scanning protocol is described in detail in the supplemental data of Appendix B.

The PET images are reconstructed using a 3-dimensional ordered-subset expectation maximization algorithm with a spatially varying point-spread function incorporating time-of-flight information (UltraHD PET). Image reconstruction is performed with 3 iterations and 21 subsets. The slice of the PET reconstructions are matched with the attenuation-corrected low-dose CT. The reconstruction includes a three-dimensional Gaussian filter kernel with a full width half maximum of 7.5 mm, a matrix size of 256x256, and a pixel size of 3.1 mm.

The CT images are acquired for attenuation correction and anatomical reference. An X-ray tube voltage is chosen using CARE kV, with a reference tube voltage of 100 kV. The tube current time product is modulated using CARE Dose4D (Siemens), and is set to 30 mA.s. The low-dose CT is reconstructed with slice thickness of 3.0 mm, field of view of 600 mm, and an increment of 1.5 mm. An additional low-dose CT reconstruction is performed using Sinogram affirmed iterative reconstruction (Safire) strength 3, slice thickness of 3.0 mm, an increment of 1.5 mm, and field of view of 500 mm.

#### Analysis of non-imaging data

The radioactivity in the blood samples are measured in a gamma-counter. The 3 mL samples taken at each time point were divided into three samples of 1 mL. The samples are counted together with an internal standard (1% of the injected dose) of the administered dose in triplicate. The activity is decay corrected to the injection time and time-activity curves are created. The activity within the blood is given as mean percentage of the injected dose per gram  $\pm$  standard deviation, calculated with the formula:  $\frac{1 \times CPM_s \times w_s}{CPM_{std}}$  (with  $w_s$  = weight of tissue sample,  $CPM_s$  = counts per minute of the sample,  $CPM_{std}$  = counts per minute of the standard). The elimination rate constant (gradient,  $k_e$ ) is determined using the curve fitting procedure in Matlab (MATLAB R2014b, The MathWorks Inc., Natick, MA). With this

gradient, the time that is required to reach half of its original value ( $t_{1/2\beta}$ ) was calculated with the formula  $\frac{\ln(2)}{k_e}$ .

#### PET/CT imaging analysis

##### Biodistribution

Visual analysis of the fused PET/CT images is performed using HERMES (Hermes Medical Solutions AB, Stockholm, Sweden). Quantitative analysis is performed using Inveon Research Workspace Software, version 4.1 (Preclinical Solutions, Siemens Medical Solutions USA, Knoxville Tennessee, USA). The mean and maximal standardized uptake values ( $SUV_{mean}$  and  $SUV_{max}$ ) are calculated according to the formula:  $SUV = \frac{A_i}{A_{inj}/w_{pt}}$ , with  $A_i$  = the (mean or max) activity within the VOI (Bq/ml),  $A_{inj}$  = decay corrected amount of injected radiolabeled RGD (Bq), and  $w_{pt}$  = the body weight of the patient (kg).

The organs of interest (lungs, heart, kidney, liver, spleen, stomach, bladder, thyroid, brain, brain ventricles, and adrenal glands) are delineated in the CT images using a manually drawn volume of interest of the whole organ (VOI) in all three planes (sagittal, coronal, and transverse). These VOIs are aligned on the PET data and  $SUV_{mean}$  and  $SUV_{max}$  within the VOIs is determined. Activity in the muscle is obtained by drawing a manually defined VOI of approximately 24 cm<sup>3</sup> in the deltoid muscle. Activity in the small and large intestines is determined by drawing three VOIs of 4 cm<sup>3</sup> that is placed at three different places within the body. Activity within the intestines is calculated as mean activity of the three regions. For the blood pool value, an ellipsoid VOI is drawn in the brachiocephalic artery, with a volume of approximately 4.5 cm<sup>3</sup>. Background activity was measured using an ellipsoidal VOI in the tongue of approximately 12 cm<sup>3</sup>.  $SUV_{mean}$  is presented as mean  $\pm$  standard deviation.

##### Tumor delineation

The tumor volume is delineated in the PET images using three methods: (1) a fixed threshold region growing segmentation method at 50% ( $SUV_{50\%}$ ), (2) a fixed threshold region growing segmentation method at 80% ( $SUV_{80\%}$ ) and (3) a fixed threshold based method representing the eight voxels surrounding the  $SUV_{max}$  ( $SUV_{peak}$ ). More information regarding these delineation methods is given in the supplementary data of Appendix B. The  $SUV_{50\%}$  and  $SUV_{80\%}$  are presented as mean  $\pm$  standard deviation. Tumor-to-blood (TBR), tumor-to-kidney (TKR), and tumor-to-muscle (TMR) ratios are calculated and given as ratio of the tumor  $SUV_{80\%}$  and non-tumor  $SUV_{mean}$ .

#### Preliminary results

So far, two patients have been included. Table 4 summarizes the patients characteristics. <sup>68</sup>Ga-DOTA-RGD<sub>2</sub> PET/CT scan was performed before surgery (5 days and 4 days before the surgery, respectively). Unfortunately, the PET/CT scan of the first patient was interrupted due to severe claustrophobia of the patient during the PET/CT scan.

#### Non-imaging data

No drug related adverse events were reported after injection of <sup>68</sup>Ga-DOTA-RGD<sub>2</sub>. Vital signs, e.g. blood pressure, heart rate, and temperature, were monitored at baseline and 120 minutes after injection. No significant changes were observed. The liver parameters (ASAT, ALAT, total bilirubin) and kidney parameters (creatinine clearance) did not show any significant short term changes. These results showed that the injection of <sup>68</sup>Ga-DOTA-RGD<sub>2</sub> did not affect kidney- or liver function of these patients, indicating a safe procedure.

**Table 4.** Demographic patient characteristics, injected dose per subject, and mean injected dose per gram  $\pm$  standard deviation (%ID/g  $\pm$  stdev) of the blood samples.

Subject	Gender	Age	Weight (kg)	TNM-stage	Location	Maximal diameter
<b>Patients characteristics</b>						
1	M	68	91	cT2N2aM0 pT4aN1aM0	Oropharynx (left tonsil) and metastatic lymph node metastases	Lymph node: 5x3 cm
2	M	69	75	cT4N0M0 pT4N2bM0	Anterior oral cavity and processus alveolaris inferior bilateral	Tumor: 5x2x7 cm
Subject	Injected dose (MBq)	%ID/g t=5 min p.i.	%ID/g t=30 min p.i.	%ID/g t=60 min p.i.	%ID/g t=90 min p.i.	%ID/g t=120 min p.i.
<b>Tracer characteristics</b>						
1	218.5	3.9 $\pm$ 0.01	1.8 $\pm$ 0.03	1.1 $\pm$ 0.03	0.7 $\pm$ 0.0	0.6 $\pm$ 0.1
2	218.3	1.9 $\pm$ 0.3	0.7 $\pm$ 0.2	0.5 $\pm$ 0.1	0.3 $\pm$ 0.1	0.2 $\pm$ 0.1

Blood sampling indicated rapid blood clearance of the radiotracer. The blood clearance curves in Figure 11 showed that after 5 minutes less than 4 %ID/g is present within the blood. Within 30 minutes, the tracer is distributed from the blood to surrounding tissue and organs. The tracer is excreted by the kidneys. After two hours less than 1 %ID/g remained in the circulation.

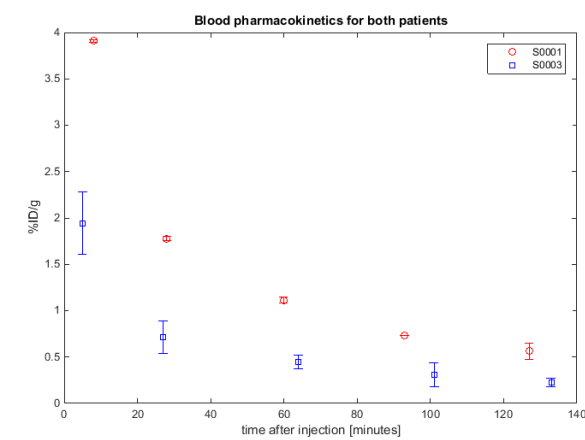
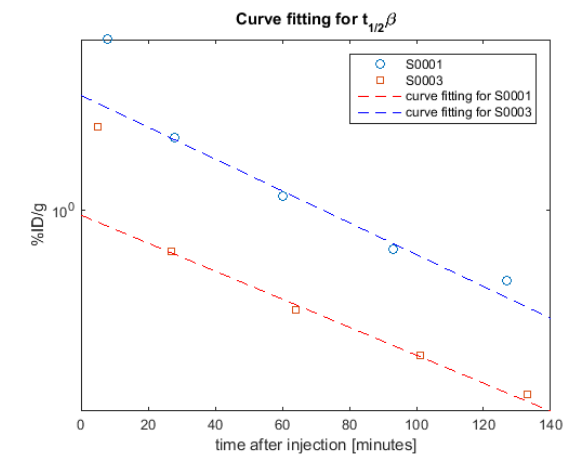
The elimination rate constant,  $k_e$  is 0.01275 min<sup>-1</sup> (95% CI: 0.01729; 0.008213) for patient 1 and 0.0112 min<sup>-1</sup> (95% CI: 0.01376; 0.008649) for patient 2. This resulted in an estimated half-life of the elimination phase ( $t_{1/2\beta}$ ) of 55 minutes for patient 1 and  $t_{1/2\beta}$  = 62 minutes for patient 2.

#### Imaging data

The tumor of the second patient was described as a HNSCC of the oral cavity, with invasion in the right jawbone and tongue. The maximal diameter of the lesion was 4.6 cm. Two pathologic lymph node metastases were found, in level II of the left neck side (diameter of 15 and 10 mm respectively). However, with the PET/CT images, these nodes could not be identified by  $^{68}\text{Ga}$ -DOTA-RGD<sub>2</sub>, probably due to the inability to distinguish these nodes from the tumor lesion or tracer uptake within the submandibular gland.

The tumor showed clear, heterogeneous accumulation of  $^{68}\text{Ga}$ -DOTA-RGD<sub>2</sub> (Figure 13). The SUV<sub>max</sub> of the tumor tissue were 5.9, 6.2, and 6.1 at 30, 60, and 90 minutes post injection (p.i.), respectively. The SUV<sub>peak</sub> were respectively 5.5, 5.7, and 6.5. The SUV<sub>50%</sub> were respectively 3.9  $\pm$  0.7, 4.0  $\pm$  0.7, and 4.0  $\pm$  0.7, and the SUV<sub>80%</sub> of tumor uptake 5.2  $\pm$  0.3, 5.3  $\pm$  0.3, and 5.3  $\pm$  0.3, respectively.

The highest uptake in non-tumor tissue was found in the bladder, in which SUV<sub>mean</sub> values were 51.9  $\pm$  24.3, 66.1  $\pm$  22.5, and 69.3  $\pm$  12.7 at 30, 60, and 90 minutes p.i., respectively. The results of both the SUV<sub>mean</sub> and SUV<sub>max</sub> measurements for all organs and non-targeted tissues, are given in Table 5. Uptake of  $^{68}\text{Ga}$ -DOTA-RGD<sub>2</sub> in non-targeting organs is illustrated in Figure 14 and was especially seen in the liver (SUV<sub>mean</sub>, 60 min p.i. 1.9  $\pm$  0.5), spleen (SUV<sub>mean</sub>, 60 min p.i. 2.1  $\pm$  1.0), and kidneys (SUV<sub>mean</sub>, 60 min p.i. 4.2  $\pm$  2.3). The large standard deviation of the kidney uptake is considered to be due to the excretion of  $^{68}\text{Ga}$ -DOTA-RGD<sub>2</sub>, and due to  $\alpha_v\beta_3$  integrin expression at the vascular endothelium and glomerular

**Figure 11.** Graphic illustration of the time-activity concentration of the blood samples as mean percentage of the injected dose per gram (%ID/g). Error bars indicate standard deviations.**Figure 12.** Graphic illustration of linear curve fitting to determine the  $t_{1/2\beta}$ . Note the semi-logarithmic y-axis.

epithelial cells of the kidneys [67]. Some focal uptake was seen in the psoriasis of the left arm, and Dupuytren grade II of the fourth metacarpal bone of the right hand (Figure 15). Note the different position of the left arm at the last scan. This was due to irritation of the elbow joint.

The biodistribution showed only moderate accumulation in non-targeted tissues. Background activity close to the tumor was seen in the submandibular glands (SUV<sub>mean</sub>, 60 min p.i.: 2.4  $\pm$  0.8) and thyroid gland (SUV<sub>mean</sub>, 60 min p.i.: 1.5  $\pm$  0.4). Because background activity close to tumor was low and rapid clearance from the blood was seen, sufficient TBR and TMR could be obtained. TBR was calculated to be 5.2  $\pm$  0.6, 6.8  $\pm$  1.1, and 8.7  $\pm$  1.3 at 30, 60, and 90 minutes p.i. respectively. The TMR was calculated to be 6.4  $\pm$  1.5, 5.6  $\pm$  2.0, and 6.3  $\pm$  2.4 respectively. The TKR was calculated to be 1.1  $\pm$  1.0, 1.3  $\pm$  0.7, and 1.5  $\pm$  0.9 respectively.

#### Immunohistochemistry

Five biopsies were taken from the fresh obtained tumor specimen: (1) left side, peripheral side of the tumor, located close to the jawbone, (2) left side, anterior part of the tumor, (3) centre of the tumor, (4) anterior right side of the tumor, 1 cm deep, and (5) right side, peripheral close to jawbone. A 2D representation of the tumor biopsy places is given in the supplementary data of Appendix B. The results of the immunohistochemistry are not yet available.

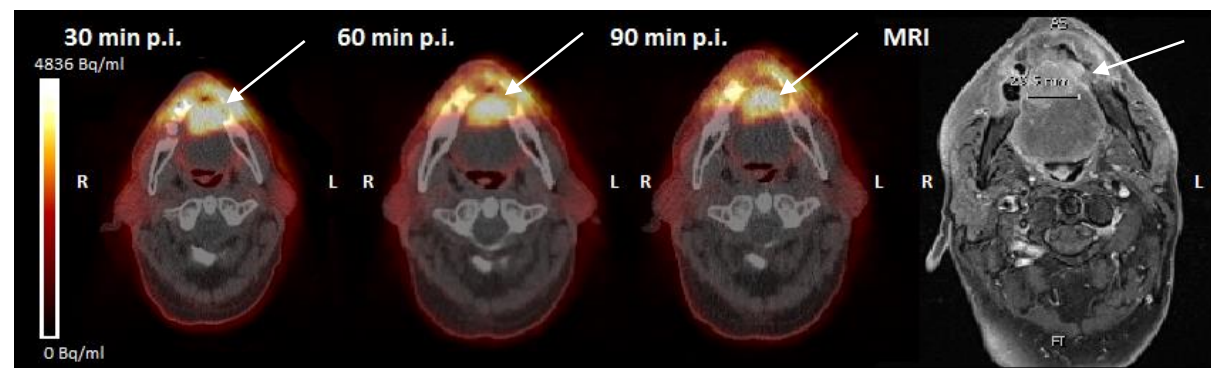


**Figure 13.** Transverse view of tumor site of patient with HNSCC of the oral cavity. Images display the three PET/CT imaging time points and the diagnostic MRI image (tumor is indicated by white arrow). Tumor showed heterogeneous uptake.

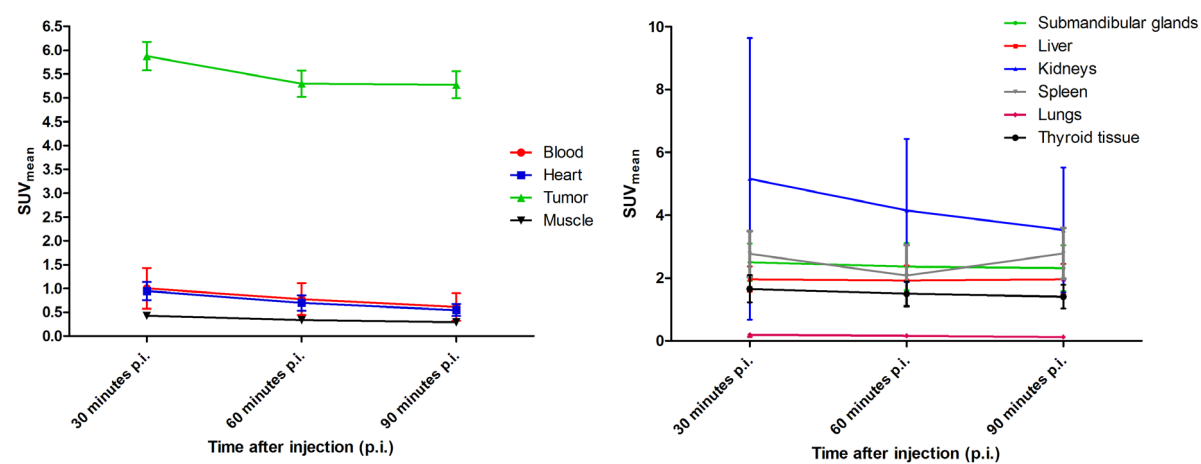


**Figure 14.** Mean SUV ± standard deviation in blood, heart, and muscle, and SUV<sub>80%</sub> (left) and submandibular glands, liver, kidneys, spleen, lungs, and thyroid tissue (right) as obtained from the PET/CT images.

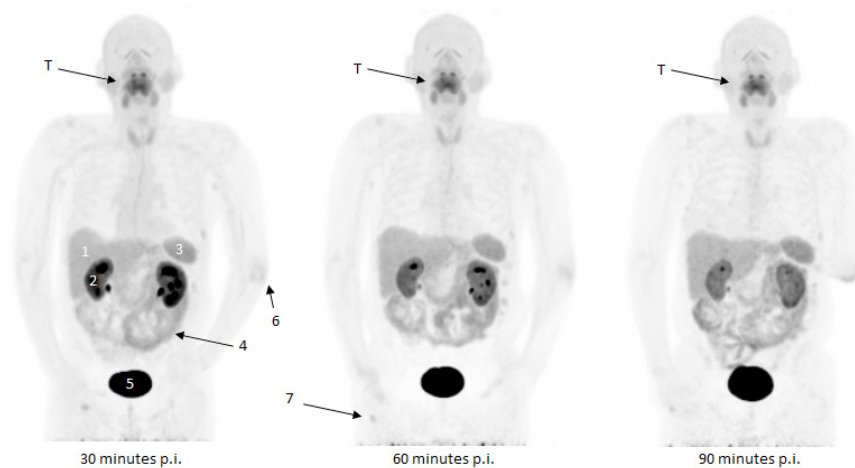


**Figure 15.** Patient with a HNSCC tumor in the oral cavity (indicated with T). The maximum intensity projections at the three imaging time points (left: 30 minutes p.i., middle: 60 minutes p.i., right: 90 minutes p.i.). Non-tumor targeting is seen in (1) liver, (2) kidneys, showing enhanced accumulation over time, partly explained by  $\alpha\beta_3$  integrin targeting on vascular endothelium and glomerular epithelial cells and due to excretion of <sup>68</sup>Ga-DOTA-RGD<sub>2</sub>, (3) spleen, (4) intestines, showing decreased activity over time, (5) bladder, (6) psoriasis of the left arm, and (7) fourth metacarpal bone of the right hand.

**Table 5.** Mean and maximal SUV ± standard deviation of organs at the three imaging time-points. \*Mean of both kidneys, #mean of three VOIs.

Organ	30 minutes p.i.		60 minutes p.i.		90 minutes p.i.	
	SUV <sub>max</sub>	SUV <sub>mean</sub>	SUV <sub>max</sub>	SUV <sub>mean</sub>	SUV <sub>max</sub>	SUV <sub>mean</sub>
Blood	1.3	1.0 ± 0.1	0.9	0.8 ± 0.1	0.8	0.6 ± 0.1
Muscle	0.7	0.4 ± 0.1	0.5	0.4 ± 0.1	0.5	0.3 ± 0.0
Heart	2.0	1.0 ± 0.2	1.5	0.7 ± 0.1	1.7	0.6 ± 0.1
Lungs	2.2	0.2 ± 0.1	0.6	0.2 ± 0.1	0.5	0.1 ± 0.1
Liver	4.0	2.0 ± 0.4	4.0	1.9 ± 0.5	4.0	2.0 ± 0.5
Spleen	4.0	2.8 ± 0.7	3.9	2.1 ± 1.0	4.3	2.8 ± 0.8
Stomach	2.7	0.7 ± 0.5	2.9	1.0 ± 0.5	3.1	0.9 ± 0.7
Kidneys*	36.8	5.2 ± 4.5	12.7	4.2 ± 2.3	7.7	3.5 ± 2.0
Bladder	85.4	51.9 ± 24.3	92.1	66.1 ± 22.5	84.7	69.3 ± 12.7
Large intestines#	2.5	1.6 ± 0.7	1.5	3.2 ± 0.6	2.0	1.2 ± 0.7
Small intestines#	2.9	2.2 ± 0.8	2.5	1.3 ± 0.9	2.6	1.8 ± 4.5
Thyroid gland	2.7	1.7 ± 0.4	2.6	1.5 ± 0.4	2.4	1.4 ± 0.4
Brain tissue	0.6	0.1 ± 0.1	0.5	0.1 ± 0.1	0.5	0.1 ± 0.1
Brain ventricles	2.6	0.4 ± 0.7	2.4	0.4 ± 0.6	2.4	0.5 ± 0.7
Submandibular gland	3.3	2.5 ± 0.6	3.2	2.4 ± 0.8	3.2	2.3 ± 0.7
Tongue	1.8	0.9 ± 0.2	2.6	1.0 ± 0.3	2.5	0.8 ± 0.3
Bone marrow	0.3	0.2 ± 0.04	0.8	0.4 ± 0.1	0.6	0.4 ± 0.1

## Discussion

The PET/CT imaging data obtained in the first patient, clearly showed accumulation of <sup>68</sup>Ga-DOTA-RGD<sub>2</sub> uptake in the tumor. Furthermore, no adverse events related to the study drug were seen. Although only preliminary results of the ongoing study can be presented, the PET/CT images showed favorable biodistribution (tracer uptake in non-tumor tissue was low), fast renal excretion (<1% ID/g in blood after 90 minutes p.i.), and good TBR and TMR ratios (>2). It cannot be stated that tracer uptake within tumor tissue was  $\alpha_v\beta_3$  integrin mediated, since the immunohistochemical findings were not available. Nevertheless, the preliminary findings were successfully translated into clinic, indicating <sup>68</sup>Ga-DOTA-RGD<sub>2</sub> PET/CT imaging in HNSCC has the potential to image  $\alpha_v\beta_3$  integrin expression.

## Comparison with literature

Aim of this ongoing study is to assess the feasibility and safety of <sup>68</sup>Ga-DOTA-RGD<sub>2</sub> PET/CT imaging in 25 HNSCC patients. However, in a recent study of López *et al.*, five healthy volunteers underwent a <sup>68</sup>Ga-DOTA-RGD<sub>2</sub> PET/CT scan to determine the dosimetry of this tracer [68]. Furthermore, no adverse events or clinically detectable pharmacologic effects were observed in their study [68]. The mean effective dose of a <sup>68</sup>Ga-DOTA-RGD<sub>2</sub> injection was estimated to be 20.9 ± 5.2  $\mu$ Sv/MBq in a one-hour-voiding model, indicating that for an administered activity of 200 MBq, the mean effective dose would be 4.2 mSv [68]. These findings are in line with the effective doses of other <sup>68</sup>Ga- and <sup>18</sup>F-labeled RGD peptides that ranged from 10-40  $\mu$ Sv/MBq [22, 26, 31, 32, 41, 69]. Our preliminary data are in line with their findings, making it even more conceivable that <sup>68</sup>Ga-DOTA-RGD<sub>2</sub> PET/CT imaging is a safe procedure.

There are several published studies in which the pharmacokinetics of RGD-based radiotracers were determined by evaluating blood samples [36, 44]. Mitra *et al.* obtained 1-mL blood samples at 10

time points after injection of  $^{18}\text{F}$ -FPPRGD<sub>2</sub> [36]. The time-activity curves showed that 90 minutes after injection only  $8 \pm 2\%$  of the tracer was present within the blood. Kenny *et al.* showed that less than 10% of the tracers was present within the blood after one hour and a biological half-life of 10 minutes was calculated [44]. Our results are in line with both studies.

The metastatic lymph nodes found in our patient were not seen with  $^{68}\text{Ga}$ -DOTA-RGD<sub>2</sub> PET/CT. One of the previous clinical studies using  $^{68}\text{Ga}$ -NOTA-PRGD<sub>2</sub> PET/CT, studied the accuracy of  $^{68}\text{Ga}$ -NOTA-PRGD<sub>2</sub> PET/CT in the detection of lymph nodes metastasis in lung cancer patients [42]. They showed significantly better positive and negative predictive values for RGD PET/CT compared to standard  $^{18}\text{F}$ -FDG PET/CT (90.0% and 93.8% versus 30.2% and 90.5%, respectively) [42]. The lymph node metastasis in our patient were not found, probably due to the close location of the lymph nodes to the submandibular glands. However, more patients are first needed to determine the positive and negative predictive values of  $^{68}\text{Ga}$ -DOTA-RGD<sub>2</sub> in the detecting of metastatic lymph nodes.

The preliminary results proved that in HNSCC  $\alpha_v\beta_3$  integrin is solely expressed on the neovasculature of the tumor, resulting in lower tracer accumulation in HNSCC tumors than tracer uptake in other types of tumors. A previous clinical study with  $^{18}\text{F}$ -Galacto-RGD PET/CT in HNSCC found a  $\text{SUV}_{\text{mean}}$  of  $3.4 \pm 1.2$  for tumor,  $1.3 \pm 0.2$  for blood, and  $1.6 \pm 0.4$  for the submandibular glands [23]. Taken the limited data of our study into account, differences between the two studies are present (tumor  $\text{SUV}_{80\%}$  of  $5.3 \pm 0.3$ ,  $\text{SUV}_{\text{mean}}$  of  $0.8 \pm 0.1$  for blood, and  $2.4 \pm 0.8$  for the submandibular glands), probably due to the use of different radiotracers, e.g. multimerization of the peptide, different used radionuclides, and chemical structure differences of both compounds. Another important factor that should be considered by comparing these two studies, is related to the different segmentation methods used. Whereas Beer *et al.* used a SUV cut-off value of 3.0, our tumor volume was estimated by  $\text{SUV}_{80\%}$ . To allow comparisons between our data and findings mentioned in literature, it is important to use identical reconstruction settings and similar quantification methods.

Enhanced uptake of  $^{68}\text{Ga}$ -DOTA-RGD<sub>2</sub> in non-tumor tissue was seen within the choroid plexus, brain ventricles, thyroid gland, and submandibular glands. Tracer accumulation in the brain ventricles is explained by the expression of  $\alpha_v\beta_3$  integrin expression on normal brain tissue [70]. Furthermore, accumulation was already seen in previous reported studies using RGD-based peptides [36, 39, 68, 71]. The uptake of  $^{68}\text{Ga}$ -DOTA-RGD<sub>2</sub> in thyroid gland is explained by the fact that  $\alpha_v\beta_3$  integrin also acts as a membrane receptor for thyroid hormones (THs) [72]. The accumulation of  $^{68}\text{Ga}$ -DOTA-RGD<sub>2</sub> in the submandibular glands is probably explained by physiological uptake. From other  $^{68}\text{Ga}$ -based radiotracers, such as  $^{68}\text{Ga}$ -PSMA (a biomarker targeting prostate-specific membrane antigens), it is known that normal distribution shows enhanced uptake in the salivary glands (parotid gland, submandibular, and lacrimal glands), due to physiologic uptake [73]. In case of  $^{68}\text{Ga}$ -DOTA-RGD<sub>2</sub>, only moderate uptake within the submandibular gland is seen. It is recommended to determine if this uptake is  $^{68}\text{Ga}$  mediated or  $\alpha_v\beta_3$  integrin mediated.

#### Method limitations and recommendations

In this study, segmentation of the tumor volume was performed using three different fixed-threshold based methods. These kind of methods can be implemented easily in clinical practice and have already been validated in several types of cancers [74, 75]. The effect of this fixed-threshold based segmentation is shown in Figure 16. Based on the anatomical information (intact left jawbone), it was suggested

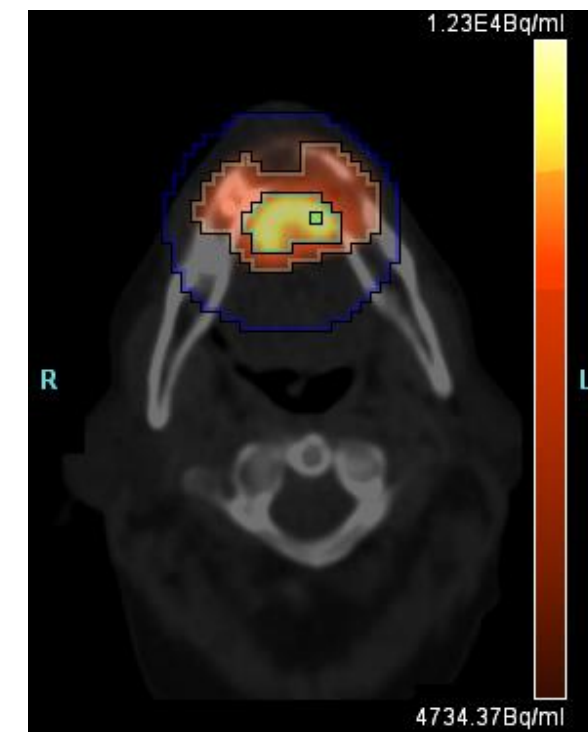


**Figure 16.** Effect of threshold-based segmentation of tumor volume. Blue circle represents the container, green box represents the seed point, light blue region is  $\text{SUV}_{80\%}$ , purple is  $\text{SUV}_{50\%}$ .

that the 80% threshold (light blue region) was a reliable threshold based segmentation method. However, the pathological findings indicated that the tumor was invaded in the right jawbone. This was confirmed by CT, in which a disrupted jawbone was seen. Based on this information, the  $\text{SUV}_{80\%}$  does not represent the true tumor volume, because tracer accumulation within the left jawbone may represent  $\alpha_v\beta_3$  integrin expression as well.

If tumor volumes within a patient are measured over time, an adequate estimate of tracer accumulation in tumor volume is needed. Because  $^{68}\text{Ga}$ -DOTA-RGD<sub>2</sub> PET/CT might be used to measure responses to therapy in the future clinical studies, reliable segmentation methods should be investigated. Therefore, it is recommended to repeat the SUV measures using different segmentation settings during this feasibility and safety study. Another segmentation method is an adaptive based threshold method. Examples of adaptive threshold based methods are segmentations based on signal-to-background ratios (SBR method) or segmentations based on a relative threshold level (RTL method) [76, 77]. Non-threshold based segmentation methods are often based on a stochastic approach. Examples of these kind of methods are fuzzy locally adaptive Bayesian algorithm (FLAB) and gradient-based methods using watershed transform algorithms and hierarchical clustering analysis [78, 79]. It goes beyond the scope of this thesis to introduce the similarities and differences and to discuss the advantages and drawbacks of these kinds of segmentation methods. Research should be conducted to indicate which segmentation method will give the most reliable and most accurate value of the tumor volume, but this will only be feasible if more patients are scanned.

The pharmacokinetic behavior of  $^{68}\text{Ga}$ -DOTA-RGD<sub>2</sub> was assessed by drawing blood samples at five different time points. With these data points, a biexponential clearance curve of tracer activity from

the blood was seen. The half life of distribution ( $t_{1/2\alpha}$ ) calculation is strongly depending on the first couple of sampling time points. Since only two data points were measured in the first couple of minutes after injection, it is recommended to choose three additional time points to determine  $t_{1/2\alpha}$  adequately. Therefore, in the following patients, additional blood samples at  $t=2$ ,  $t=4$ , and  $t=10$  are drawn.

### Conclusion

This study is the first clinical imaging study using  $^{68}\text{Ga}$ -DOTA-RGD<sub>2</sub> PET/CT to image  $\alpha_v\beta_3$  integrin expression in HNSCC. The preliminary findings in the first patients showed the potential of  $^{68}\text{Ga}$ -DOTA-RGD<sub>2</sub> PET/CT in HNSCC as the tumor clearly showed increased targeting compared to surrounding tissues. Imaging of more patients is needed to determine the feasibility and safety of  $^{68}\text{Ga}$ -DOTA-RGD<sub>2</sub> as tracer to image  $\alpha_v\beta_3$  integrin in tumor lesions and to validate whether the tracer uptake within tumor tissue is  $\alpha_v\beta_3$  integrin mediated. However, it is recommended to optimize the delineation method of the tumor volume during the current study.

## Appendix A. Approval of the Medical Ethical Committee for the 'RGD PET' study, correspondence number: NL52649.091.15 (2015-1813)

# Radboudumc

Radboud universitair medisch centrum  
Concernstaf Kwaliteit en Veiligheid  
Commissie Mensgebonden Onderzoek  
Regio Arnhem-Nijmegen

Postbus 9101, 6500 HB Nijmegen  
Huispost 628  
Geert Grooteplein 10  
Radboudumc hoofdingang, route 627  
T (024) 361 31 54

cmo@iwkv.umcn.nl  
KvK 41055629/4

628

Mw. D. Lobeek  
756 Radiologie en Nucleaire Geneeskunde  
Radboudumc

Ons Kenmerk  
DS/CMO 314

Datum  
28 juli 2015

**Titel:** Ga-68-DOTA-RGD2 PET in patients with head and neck cancer: a potential tracer to image angiogenesis in tumors  
**Dossiernummer:** 2015-1813  
**NL-nummer:** NL52649.091.15

Geachte mevrouw Lobeek,

Bijgevoegd treft u aan het positieve oordeel van de CMO Regio Arnhem-Nijmegen over bovengenoemd onderzoek.

Dit betekent dat het onderzoek kan worden uitgevoerd in het centrum dat in het positieve oordeel wordt genoemd nadat de Raad van Bestuur/Directie van het centrum daarvoor toestemming heeft verleend.

Indien het voornemen bestaat het onderzoek ook nog in een ander centrum uit te voeren, dan dient aan de CMO Regio Arnhem – Nijmegen een onderzoeksverklaring (zie website [www.ccmo.nl](http://www.ccmo.nl)) van het betreffende centrum te worden overlegd. De CMO Regio Arnhem-Nijmegen kan vervolgens het positieve oordeel uitbreiden naar het betreffende centrum.

### **Nota bene!**

Voorwaarde voor het uitvoeren van een WMO-onderzoek in het Radboudumc is niet alleen het positieve oordeel van de CMO regio Arnhem-Nijmegen (of een andere erkende METC) maar ook de toestemming van de Raad van Bestuur van het Radboudumc. Om deze vereiste toestemming te verkrijgen, moet u uw onderzoek aanmelden bij het servicepunt CRCN (huispost 392, tel: (024) 36 68333), die een en ander coördineert.

Bij correspondentie over het onderzoek gelieve titel en dossiernummer te vermelden.



Kamer van Koophandel - handelsregister 41055629

## Radboudumc

Ik vertrouw erop u met dit schrijven van dienst te zijn en namens de commissie wens ik u succes met de uitvoering van het onderzoek.

Met vriendelijke groet,  
Namens de CMO Regio Arnhem-Nijmegen



Mw. dr. M. Verlaan, secretaris

Positief besluit NL52649.091.15, 28072015

Kamer van Koophandel - handelsregister 41055629



Pagina 2 van 8

## Radboudumc

BESLUIT  
Primaire beoordeling

NL nummer:	52649.091.15	METC nr.	2015-1813
Titel onderzoek:	Ga-68-DOTA-RGD2 PET in patients with head and neck cancer: a potential tracer to image angiogenesis in tumors		

Contactgegevens: Mw. D. Lobeek, 756 Radiologie en Nucleaire Geneeskunde  
Verrichter: Radboudumc te Nijmegen

### Besluit

De medisch-ethische toetsingscommissie CMO Regio Arnhem-Nijmegen heeft zich, op grond van artikel 2, tweede lid, sub a van de *Wet medisch wetenschappelijk onderzoek met mensen (WMO)*, beraden over bovenstaand onderzoeksdossier.

De commissie oordeelt positief over het onderzoeksdossier uit te voeren in het volgende centrum:  
- Radboudumc te Nijmegen (hoofdonderzoeker prof. dr. W. Oyen)

In dit onderzoek worden maximaal 25 proefpersonen geïnccludeerd. Bestaat het voornemen het totaal aantal proefpersonen te wijzigen dan moet dat ter beoordeling aan de commissie worden voorgelegd.

### Documenten

Het oordeel is gebaseerd op de documenten die in [bijlage 1](#) zijn vermeld.

### Achtergrond

Op 13 mei 2015 is het onderzoeksdossier ter beoordeling bij de commissie ingediend (na ontvangst van de ontbrekende stukken, was het dossier compleet aangeleverd d.d. 21 juli 2015). Met inachtneming van haar reglement is het onderzoeksdossier besproken in de vergadering van 2 juni 2015; zie [bijlage 2](#) voor de bij de beoordeling betrokken commissieleden.

### Overwegingen

De commissie is van oordeel dat aan de voorwaarden in artikel 3 van de WMO is voldaan.

De commissie heeft de inhoud van de onderzoeksverklaring van de deelnemende instelling bekeken. Zij heeft geconstateerd dat is voldaan aan de voorwaarden in artikel 3, onderdeel e en j, van de WMO.

Naar de mening van de commissie betreft het geneesmiddelenonderzoek zoals bedoeld in artikel 1, eerste lid onder n, van de WMO. Tevens is artikel 13a van de WMO van toepassing en is voldaan aan alle in artikel 13d van de WMO genoemde aanvullende voorwaarden.

De commissie is van oordeel dat het onderzoeksprotocol in een toestemmingsprocedure voorziet die overeenstemt met artikel 6, eerste lid, van de WMO.

Positief besluit NL52649.091.15, 28072015

Kamer van Koophandel - handelsregister 41055629



Pagina 3 van 8

## Radboudumc

De commissie is van mening dat is voldaan aan de voorwaarden in artikel 6, vijfde t/m negende lid, van de WMO. De proefpersonen (en/of degenen die mede/in hun plaats bevoegd zijn tot het geven van toestemming voor deelname aan het onderzoek) worden op gepaste, volledige en begrijpelijke wijze schriftelijk over het onderzoek geïnformeerd.

### Verzekeringen

De commissie heeft geconstateerd dat is voldaan aan de verzekeringsplicht. Er is een proefpersonenverzekering afgesloten zoals bepaald in artikel 7, eerste lid, van de WMO en zoals nader uitgewerkt in het Besluit verplichte verzekering bij medisch-wetenschappelijk onderzoek met mensen 2015 (Besluit van 24 november 2014).

Het onderzoek valt onder de proefpersonenverzekering van het Radboudumc.

De commissie heeft geconstateerd dat een aansprakelijkheidsverzekering is afgesloten zoals bepaald in artikel 7, negende lid, van de WMO.

Ten slotte wijst de commissie u op de voorwaarden en verplichtingen die in bijlage 3 zijn vermeld.

Hoogachtend,  
Namens de CMO Regio Arnhem-Nijmegen



Dr. M.J.J. Prick, vicevoorzitter

Nijmegen, 28 juli 2015

### Beroepsprocedure

Tegen dit besluit kan een belanghebbende op grond van artikel 23 van de WMO binnen zes weken na de dag waarop het besluit is bekend gemaakt, administratief beroep instellen bij de Centrale Commissie Mensgebonden Onderzoek (CCMO). Het beroepschrift dient u te adresseren aan CCMO, Postbus 16302, 2500 BH Den Haag.



## Radboudumc

### Bijlage 1

#### Documenten:

- A Aanbiedingsbrief van prof. dr. W. Oyen en mw. D. Lobeek d.d. 8 mei 2015 (alhier ontvangen d.d. 13 mei 2015)  
Overzicht ingediende documenten  
Ontvangstbewijs EudraCt-nummer d.d. 19 februari 2015  
Brief van prof. dr. W. Oyen en mw. D. Lobeek d.d. 3 juli 2015 (in antwoord op commissieschrijven d.d. 4 juni 2015)  
Brief van prof. dr. W. Oyen en mw. D. Lobeek d.d. 21 juli 2015 (in antwoord op commissieschrijven d.d. 20 juli 2015)
- B ABR-formulier, versie 2 d.d. 13 mei 2015  
EudraCt formulier d.d. 11 mei 2015
- C Onderzoeksprotocol, versie 2, d.d. 3 juli 2015
- D Investigator's Brochure, versie 1 d.d. 7 mei 2015  
Voorbeeldetiket Spuit  
Voorbeeldetiket Flacon  
Voorbeeldetiket verpakkingdoos  
Fabrikantenvergunning apotheek  
Bereidingsvoorschrift d.d. 8 oktober 2012  
Labelingsvoorschrift, versie 1 d.d. 12 september 2014  
IMPD RGD-DOTA, versie 2 d.d. 18 februari 2014  
IMPD Ga68-RGD-DOTA, versie 1 d.d. 7 april 2014
- E Proefpersoneninformatie incl. toestemmingsformulier deelstudie A, versie 3 (ongedateerd, ontvangen d.d. 21 juli 2015)  
Proefpersoneninformatie incl. toestemmingsformulier deelstudie B, versie 3 (ongedateerd, ontvangen d.d. 21 juli 2015)  
Proefpersoneninformatie incl. toestemmingsformulier deelstudie C, versie 3 (ongedateerd, ontvangen d.d. 21 juli 2015)
- G Certificaat WMO proefpersonenverzekering van Radboudumc (datum afgifte CRCN 20 juli 2015)  
Bewijs dekking aansprakelijkheid van Radboudumc, d.d. juli 2015
- H CV onafhankelijk arts mw. I. Desar  
CV dhr. O. Boerman
- I Onderzoeksverklaring van Radboudumc, getekend d.d. 11 mei 2015, inclusief: CV prof. dr. W. Oyen
- K Radiation Ethics Form, versie 1.0



# Radboudumc

## Bijlage 2

### CMO Regio Arnhem-Nijmegen

#### Bij de beoordeling betrokken commissieleden

Voorzitter:	M. Prick
Jurist:	F. van Agt
Ethica/ethicus:	M. Roovers
Apotheker:	S. Natsch
Methodoloog:	T. Feuth
Klin.Farmacoloog:	K. Kramers
Ledenlid:	L. Bunt
Verpleegkundige:	S. Bossmann
Arts:	J. Roukema
Arts:	R. Keus



# Radboudumc

## Bijlage 3

### Voorwaarden en verplichtingen\*

- **geen bezwaar bevoegde instantie [alleen bij geneesmiddelenonderzoek]:** er kan pas met het onderzoek worden gestart, wanneer eveneens geen bezwaar wordt gemaakt binnen de voorgeschreven termijn door de bevoegde instantie;
- **geldigheid oordeel:** het positieve oordeel verliest zijn geldigheid als met het onderzoek niet is gestart binnen een jaar nadat dit besluit is genomen;
- **amendementen:** amendementen dienen ter beoordeling aan de CMO Regio Arnhem-Nijmegen te worden voorgelegd;
- **startdatum onderzoek:** de CMO Regio Arnhem-Nijmegen dient op de hoogte te worden gesteld van de definitieve startdatum van het onderzoek. Dat is de datum waarop de inclusie van de eerste proefpersoon heeft plaatsgevonden;
- **voortgangsrapportage:** één jaar na de startdatum, en ieder jaar daaropvolgend, dient de METC op de hoogte te worden gebracht van de voortgang van de studie middels het formulier 'Voortgangsrapportage';
- **geldigheid verzekering:** in het geval het verzekeringscertificaat tijdens de voortgang van het onderzoek zijn geldigheid verliest, dient aan de CMO Regio Arnhem-Nijmegen tijdig een afschrift van een nieuw geldig certificaat te worden toegestuurd;
- **melding artikel 10:** indien het onderzoek een verloop neemt dat in noemenswaardige mate voor de proefpersoon ongunstiger is dan in het onderzoeksdossier is voorzien, moet daarvan terstond mededeling worden gedaan aan de CMO Regio Arnhem-Nijmegen met een verzoek tot een nader oordeel;
- **melding SAE's** SAE's dienen aan de CMO Regio Arnhem-Nijmegen gemeld te worden (raadpleeg de website van de commissie voor de te volgen procedure).
- **melding SUSAR's en jaarlijkse veiligheidsrapportage [alleen bij geneesmiddelenonderzoek]:** SUSAR's en jaarlijkse veiligheidsrapportage dienen aan de CMO Regio Arnhem-Nijmegen gemeld te worden (raadpleeg de website van de commissie voor de te volgen procedure).



## Radboudumc

- **Advies DSMB [alleen indien een DSMB is ingesteld]**  
indien een advies van de DSMB niet volledig wordt opgevolgd, dient de CMO Regio Arnhem-Nijmegen het advies met toelichting over het niet (volledig) opvolgen van het advies te ontvangen en toestemming te geven voor voortzetting van het onderzoek;
- **melding (voortijdige) beëindiging:**  
(voortijdige) beëindiging van het onderzoek dient, met redenen omkleed, te worden gemeld aan de CMO Regio Arnhem-Nijmegen.
- **eindrapportage:**  
de CMO Regio Arnhem-Nijmegen dient op de hoogte te worden gebracht van de resultaten van het onderzoek middels een eindrapport / (gesubmitte) publicatie.

\* Termijnen en overige uitleg ten aanzien van de indiening van de verschillende documenten aan de CMO Regio Arnhem-Nijmegen vindt u op de website van de CCMO bij het standaard onderzoeksdossier en de toelichting daarop en onder stap 4 van het Stappenplan toetsing TC

Positief besluit NL52649.091.15, 28072015

Kamer van Koophandel - handelaarsregister 41055629



Pagina 8 van 8

## Appendix B: Supplementary data

### Preparation of <sup>68</sup>Ga-DOTA-RGD<sub>2</sub>

The compound DOTA-RGD<sub>2</sub> was synthesized at the Department of Medicinal Chemistry and Chemical Biology of Utrecht University, Utrecht, The Netherlands, and was supervised and verified by the Department of Clinical Pharmacy of the Radboud University Medical Center, Nijmegen, the Netherlands. The product was vialled under GMP conditions to a final concentration of 70 µg/ml in 0.5 ml.

The radiolabeling of DOTA-RGD<sub>2</sub> with <sup>68</sup>Ga is performed using an <sup>68</sup>Ge/<sup>68</sup>Ga generator (Eckhardt and Ziegler, Berlin, Germany) and an automated Scintomics module (Synthesizer GRP System, typenr. 45585, Scintomics, Germany). <sup>68</sup>Ga is eluted using 10 mL 0.1N HCl and trapped on a PS-H<sup>+</sup> cartridge. Subsequently, the <sup>68</sup>Ga is eluted from the cartridge with 1.5 mL 5M NaCl into the reaction vial. In the reaction vial 0.5 mg DOTA-RGD<sub>2</sub> and 3.0 mL 1M HEPES buffer are added and the reaction mix will be heated to 100 °C for 15 minutes. After incubation, the vessel is cooled and <sup>68</sup>Ga-DOTA-RGD<sub>2</sub> is purified (within the module) using a Seppak C18 plus cartridge and eluted from the cartridge using a 5% ethanol solution (2 ml). Subsequently, this solution is further diluted with 20 ml phosphate buffered saline solution. After synthesis of <sup>68</sup>Ga-DOTA-RGD<sub>2</sub>, quality control of each preparation is performed before release of <sup>68</sup>Ga-DOTA-RGD<sub>2</sub>. The radiochemical purity is tested using ITLC and RP-HPLC. After labeling, <sup>68</sup>Ga-DOTA-RGD<sub>2</sub> is stored at room temperature for patient administration. <sup>68</sup>Ga-DOTA-RGD<sub>2</sub> is injected after release by the Clinical Pharmacy, based on manufacturing data and quality control results.

### PET/CT imaging protocol

#### Study cohort A

All patients receive three static whole-body PET/CT scans, acquired from base of skull to greater trochanter. This includes 5 to 6 bed positions per subject. The PET/CT scans are performed according to the following clinical protocol: head first, supine position, arms along the body. A low-dose CT scan without contrast agent is used for anatomical identification and attenuation correction. This scan is acquired before the start of each PET scan. PET images are acquired using 4 minutes per bed position. Total scan time of one PET/CT is approximately 20 minutes.

#### Study cohort B

The CT image for attenuation correction and anatomical reference will be acquired before the PET image. A x-ray tube voltage with CARE kV, a reference tube voltage of 120 kV, and tube current modulated using CARE Dose4D (Siemens), with a reference tube current of 40 mAs, is acquired.

The <sup>68</sup>Ga-DOTA-RGD<sub>2</sub> is administered intravenously with a remote controlled syringe pump during 1 minute at the start of the PET scan. Afterwards, the system will be flushed with saline 8 mL/s for 5 seconds. The residual activity within the syringe is measured to correct for the administered activity. A venous plasma sample will be obtained at 60 minutes after injection to enable correction of the image derived arterial input function. This sample is measured in the gamma-counter together with a sample as internal standard (1% standard of the administered activity).

PET data will be acquired in list-mode setting, enabling time framing and image reconstruction. The frames sampling should be chosen according to the pharmacokinetic behaviour of the tracer. Mostly, this results in finer time sampling early after injection and wider time frames at later time points, because

the blood and tissue concentration of the radiotracer changes most rapidly early after injection. For RGD-based radiotracers this was already shown by Beer *et al.*, in which a peak blood plasma concentration of  $^{18}\text{F}$ -Galacto-RGD was seen within 10 minutes [24]. A typical time sequence used in dynamic  $^{18}\text{F}$ -FDG PET/CT images for an one minute infusion time is 15×5s, 5×15s, 5×30s, 4×1min, 4×3min and 9×5min time frames. In a study of Disselhorst *et al.*, the influence of framing schedule on the parameters was investigated [80]. They determined that as long as the initial frame durations and number of frames are chosen correctly, the method to determine the optimal framing does not influence the parameters significantly. In this study, several time framings will be acquired to determine the optimal framing schedule for  $^{68}\text{Ga}$ -DOTA-RGD<sub>2</sub>.

#### Study cohort C

PET and CT images are acquired at the optimal time point as determined in the first ten patients. This time point need to be obtained first. Patients are scanned in 1-2 bed positions covering the tumor lesion area. PET images are acquired using 4 minutes per bed position. The PET/CT scan is performed according to the following clinical protocol: head first, supine position, arms along the body. A low-dose CT scan without contrast agent is used for anatomical identification and attenuation correction. This scan is acquired before the start of the PET scan. Total scan time of the PET/CT is approximately 10 minutes.

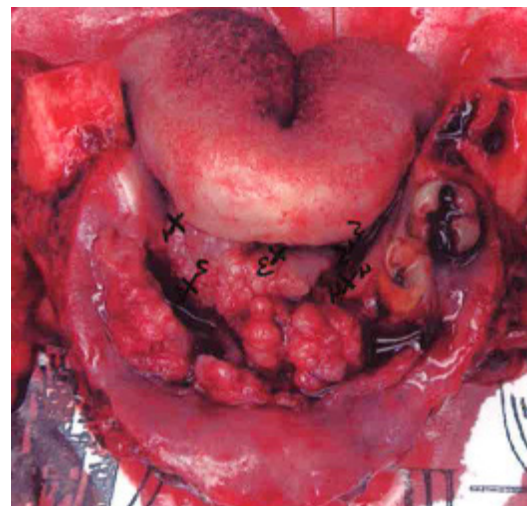
#### Tumor delineation

The tumor volume is delineated in the PET images using the following methods. The fixed threshold region growing segmentation method at 50% ( $\text{SUV}_{50\%}$ ) and 80% ( $\text{SUV}_{80\%}$ ) were obtained with the Inveon Research Workspace Software, version 4.1 (Preclinical Solutions, Siemens Medical Solutions USA, Knoxville Tennessee, USA). Therefore, a VOI (or container) in the oral cavity was placed including the whole tumor volume. The seed-point was defined as the hottest voxel ( $\text{SUV}_{\text{max}}$ ) within this container and expressed in  $\text{Mq}/\text{mL}$ . The threshold-based segmentations were subsequently applied to obtain a 50% and 80% isocontour volume of the tumor. The  $\text{SUV}_{50\%}$  and  $\text{SUV}_{80\%}$  were calculated according to the formula as described before.

The information from the container was subsequently exported to Matlab (MATLAB R2014b, The MathWorks Inc., Natick, MA). A manually built Graphic User Interface generated the  $\text{SUV}_{\text{max}}$  and subsequently created a sphere of which the volume represent  $1\text{ cm}^3$  (9 voxels) as closely as possible to the  $\text{SUV}_{\text{max}}$ . The calculated  $\text{SUV}_{\text{max}}$  was checked for conformity with the  $\text{SUV}_{\text{max}}$  as obtained previously. The  $\text{SUV}_{\text{peak}}$  was calculated according to the formula as described before.

#### Immunohistochemistry findings

A two dimensional representation of samples taken for immunohistochemistry. Biopsy samples were taken at: (1) left side, peripheral side of the tumor, located close to the jawbone, (2) left side, anterior part of the tumor, (3) centre of the tumor, (4) anterior right side of the tumor, 1 cm deep, and (5) right side, peripheral close to jawbone.



## Chapter 4: General conclusion and future perspectives

Potential radiotracers to image  $\alpha_v\beta_3$  integrin expression are often tested in xenograft tumor models that express  $\alpha_v\beta_3$  integrin on both tumor endothelial cells as well as on endothelial cells of the neovasculature (e.g. SK-RC-52 and Melanoma M21). This results in higher uptake levels of the radiotracer, suggesting that the radiotracer has potential to image  $\alpha_v\beta_3$  integrin expression with good tumor-to-background ratios. However, in tumors that do not express  $\alpha_v\beta_3$  integrin, like most head and neck cancer xenograft models, a four-fold lower tumor uptake value was found, indicating differences in  $\alpha_v\beta_3$  integrin expression between tumor types [50]. These  $\alpha_v\beta_3$  integrin negative tumors are particularly interesting to study the potential of RGD-based radiotracers to image angiogenesis, as the feasibility for PET/CT imaging of angiogenesis can only be shown when tumor cells themselves do not express  $\alpha_v\beta_3$  integrin. Therefore, the head and neck cancer cell line, such as FaDu, is more suitable to study the *in vivo* characteristics and potential for imaging angiogenesis with  $^{68}\text{Ga}$ -DOTA-RGD<sub>2</sub> PET/CT [50].

PET/CT imaging of  $\alpha_v\beta_3$  integrin expression as a non-invasive marker of angiogenesis has been widely recognized and is now subject of intensive research. Until now, eight RGD-based PET tracers and two RGD-based SPECT tracers have been investigated in clinical trials and dozens of RGD-based radiotracers have been investigated in preclinical studies. A successful RGD-based tracer to image angiogenesis should at least meet the following criteria: (1) the RGD peptide should be labeled rapidly and sufficiently with a radioisotope, (2) the radionuclide should have excellent physical characteristics (short half-life and high positron yield in case of PET imaging), (3) the tracer should be kinetically stable, (4) the chemical structure of a RGD-based radiotracer should allow  $\alpha_v\beta_3$  integrin targeting, and (5) for clinical practice the tracer should have a fast renal or hepatic excretion to reduce radiation burden to non-targeting tissue. It has been proven that  $^{68}\text{Ga}$ -DOTA-RGD<sub>2</sub> meets all criteria, making it an attractive radiotracer to apply in humans. The preclinical experiments conducted in this thesis showed that  $^{68}\text{Ga}$ -DOTA-RGD<sub>2</sub> is a viable radiotracer to image  $\alpha_v\beta_3$  integrin expression in animal models and has the potential to be used in clinic.

Much effort was taken to translate  $^{68}\text{Ga}$ -DOTA-RGD<sub>2</sub> PET/CT to clinical practice.  $^{68}\text{Ga}$ -DOTA-RGD<sub>2</sub> first underwent extensive investigation of the quality, manufacturing process and quality control process, of which the results were described in an Investigational Medicinal Product Dossier (IMPD). Second, a clinical study protocol to assess the feasibility and safety of  $^{68}\text{Ga}$ -DOTA-RGD<sub>2</sub> PET/CT imaging in HNSCC was realized. Both a dynamic and static PET/CT scan protocol are going to be applied to assess biodistribution, kinetics, and dynamics of the  $\alpha_v\beta_3$  integrin targeting characteristics in HNSCC patients. The first preliminary results showed that it is feasible and safe to administer  $^{68}\text{Ga}$ -DOTA-RGD<sub>2</sub> to HNSCC patients and that the tracer accumulates in tumor tissue. However, whether the PET/CT findings correspond with  $\alpha_v\beta_3$  integrin expression as determined by immunohistochemistry needs to be confirmed in subsequent analyses of the tumor tissue samples. Subsequently, the added value of  $^{68}\text{Ga}$ -DOTA-RGD<sub>2</sub> PET/CT for HNSCC patients could be determined by assessing its role in the diagnosis, in treatment selection or adaptation, in treatment response evaluation, or in case of the assessment of tumor recurrence during the follow-up period.

#### Future prospects

In the current guidelines for treatment of HNSCC, treatment decisions are not based on the images of molecular and functional non-invasive techniques, but rely on the immunohistological findings of biopsies. The ideal situation and the true benefit of  $^{68}\text{Ga}$ -DOTA-RGD<sub>2</sub> PET/CT within the field of

HNSCC might only realize its role in treatment adaptation in the early phase of therapy or as response monitoring tool after treatment.

#### *Treatment response monitoring tool*

A possible application of  $^{68}\text{Ga}$ -DOTA-RGD<sub>2</sub> PET/CT might be its role as a response monitoring tool after treatment. Traditional imaging techniques, such as CT and MRI, are often used to image post-treatment response, but it is challenging to make true distinctions between post-treatment changes, e.g. edema, inflammation, and fibrosis, and tumor recurrence. The role of  $^{18}\text{F}$ -FDG PET/CT is also limited for this purpose, because of its low specificity in HNSCC [81] and is only used for complement information besides standard diagnostics, e.g. physical examination and CT or MRI findings. These limitations have led to the development and evaluation of more specific molecular non-invasive imaging methods to monitor tumor response to therapy [82], including  $^{18}\text{F}$ -MISO and  $^{18}\text{F}$ -FASA (markers to bind hypoxic cells), and  $^{18}\text{F}$ -FLT (marker to measure tumor cell proliferative activity) [83]. These markers all showed the potential for use in clinic and a few clinical trials showed its value as predictive and prognostic marker in treatment response monitoring [83, 84]. In HNSCC, angiogenic factors reflect the aggressiveness and metastatic spread of tumor cells. Targeted drugs showed improved locoregional and distant control, a higher progression-free survival rate and less cancer mortality [8], making it an attractive tool for response monitoring. RGD-based radiotracers are not yet used for treatment response evaluation in HNSCC, but its role in rectal cancer was investigated. Withofs *et al.* conducted a treatment response PET/CT study with the tracer  $^{18}\text{F}$ -FPRGD<sub>2</sub> [37]. They studied the differences in  $^{18}\text{F}$ -FPRGD<sub>2</sub> uptake in locally advanced rectal cancer patients and found a significant difference ( $p=0.013$ ) between SUV<sub>max</sub> measurements for the responders group compared to the non-responders group (SUV<sub>max</sub>  $6.2\pm 1.1$  and  $4.8\pm 1.1$  respectively). However, they did not observe a correlation between SUV<sub>max</sub> before and after treatment. Whereas preclinical findings suggest the feasibility of  $^{68}\text{Ga}$ -DOTA-RGD<sub>2</sub> PET/CT as imaging tool to evaluate response to therapy, more preclinical and clinical studies need to be conducted to confirm these findings [51, 85]. Furthermore, the role of RGD-based radiotracers in post-treatment evaluation should be investigated for each tumor type separately. Until now, the results of all studies are contradictory, mainly because of the small number of patients used within these clinical trials, and because of the variation in methodological and analytical set-up of the preclinical studies.

#### *Early phase response monitoring*

Assessment of treatment efficacy in patients with HNSCC is usually measured as disease free survival rates (without tumor recurrence). Every patient currently receives the same radiotherapy treatment, sometimes in addition to chemotherapy. To prevent unnecessary ineffective therapies, the effect of therapy could be measured at an earlier time point. Only two clinical studies are available in which the potential of RGD-based radiotracers in early phase response monitoring was studied. Jaguru *et al.* studied the  $^{18}\text{F}$ -FPPRGD<sub>2</sub> uptake changes in recurrent GBM that were treated with concurrent chemoradiotherapy (bevacizumab) [33]. Despite the limited number of patients, the SUV<sub>max</sub> measurements one week after start of treatment seemed to show that the patients with only a small decrease in  $^{18}\text{F}$ -FPPRGD<sub>2</sub> uptake (less than 15% decrease) tend to have a poor prognosis, compared to the patients with a higher decrease of  $^{18}\text{F}$ -FPPRGD<sub>2</sub> uptake (more than 50% decrease). In another study with  $^{18}\text{F}$ -AIF-NOTA-PRGD<sub>2</sub> PET/CT it was demonstrated that a correlation between volumetric changes and  $^{18}\text{F}$ -AIF-NOTA-PRGD<sub>2</sub> uptake changes was present within the third week of treatment [47]. However, no correlation between standard clinical outcome measures (Response Assessment in Neuro-Oncology Criteria) and  $^{18}\text{F}$ -AIF-NOTA-PRGD<sub>2</sub> uptake with patients with newly diagnosed GBM was found [47, 86].

Analysis using follow-up data after end of treatment would give additional support of these findings. The potential use of  $^{68}\text{Ga}$ -DOTA-RGD<sub>2</sub> PET/CT imaging in early phase response monitoring or in prediction of therapy response needs further investigation. Therefore, adequate and well-defined protocols are needed and endpoints should be clearly defined. The full potential of  $^{68}\text{Ga}$ -DOTA-RGD<sub>2</sub> PET/CT as non-invasive imaging tool is yet to be determined, but changes in tracer uptake can reflect tumor response to several kinds of therapy as observed in preclinical studies [87]. We plan to conduct an observational trial to investigate the added value of therapy response monitoring in HNSCC patients, by measuring  $^{68}\text{Ga}$ -DOTA-RGD<sub>2</sub> uptake at baseline, 1-2 weeks after therapy initiation, at the end of therapy, and measure clinically relevant outcome measures such as volumetric tumor changes, morbidity, and mortality. If successful,  $^{68}\text{Ga}$ -DOTA-RGD<sub>2</sub> PET/CT can be added to standard clinical work-up of HNSCC patients.

#### **Concluding remarks**

Effective ways to non-invasively monitor treatment response or predict therapy response of anti-angiogenic therapies are needed to offer HNSCC patients more individualized therapies. A promising non-invasive imaging technique is  $^{68}\text{Ga}$ -DOTA-RGD<sub>2</sub> PET/CT and the preliminary results of this thesis support its feasibility. More patients are needed to fully evaluate the feasibility and safety of  $^{68}\text{Ga}$ -DOTA-RGD<sub>2</sub> PET/CT in HNSCC. Then,  $^{68}\text{Ga}$ -DOTA-RGD<sub>2</sub> PET/CT as tool for treatment adaptation, early response monitoring, or treatment response monitoring will be sufficiently validated.

## Bibliography

1. Nederland, I.-I.K. *Cijfers over kanker*. 2015; Available from: <http://cijfersoverkanker.nl>.
2. Torre, L.A., et al., *Global cancer statistics, 2012*. CA Cancer J Clin, 2015. **65**(2): p. 87-108.
3. Goldenberg, D., et al., *Habitual risk factors for head and neck cancer*. Otolaryngol Head Neck Surg, 2004. **131**(6): p. 986-93.
4. Braakhuis, B.J., C.R. Leemans, and O. Visser, *Incidence and survival trends of head and neck squamous cell carcinoma in the Netherlands between 1989 and 2011*. Oral Oncol, 2014. **50**(7): p. 670-5.
5. Zhu, Y., et al., *Targeting DNA repair pathways: a novel approach to reduce cancer therapeutic resistance*. Cancer Treat Rev, 2009. **35**(7): p. 590-6.
6. Hoogsteen, I.J., et al., *The hypoxic tumour microenvironment, patient selection and hypoxia-modifying treatments*. Clin Oncol (R Coll Radiol), 2007. **19**(6): p. 385-96.
7. Ridge, J.A., ; Mehra, R.; Lango, M.N.; Feigenberg, S., *Head and Neck Tumors*, in *Cancer Network home of the journal Oncology*, C. Management, Editor. 2014.
8. Blanchard, P., et al., *Chemotherapy and radiotherapy in nasopharyngeal carcinoma: an update of the MAC-NPC meta-analysis*. Lancet Oncol, 2015. **16**(6): p. 645-55.
9. Begg, A.C., F.A. Stewart, and C. Vens, *Strategies to improve radiotherapy with targeted drugs*. Nat Rev Cancer, 2011. **11**(4): p. 239-53.
10. Dorsey, K. and M. Agulnik, *Promising new molecular targeted therapies in head and neck cancer*. Drugs, 2013. **73**(4): p. 315-25.
11. Hanahan, D. and R.A. Weinberg, *The hallmarks of cancer*. Cell, 2000. **100**(1): p. 57-70.
12. Hanahan, D. and R.A. Weinberg, *Hallmarks of cancer: the next generation*. Cell, 2011. **144**(5): p. 646-74.
13. Weis, S.M. and D.A. Cheresh, *Tumor angiogenesis: molecular pathways and therapeutic targets*. Nat Med, 2011. **17**(11): p. 1359-70.
14. Carmeliet, P., *Mechanisms of angiogenesis and arteriogenesis*. Nat Med, 2000. **6**(4): p. 389-95.
15. Bergers, G. and L.E. Benjamin, *Tumorigenesis and the angiogenic switch*. Nat Rev Cancer, 2003. **3**(6): p. 401-10.
16. Weis, S.M. and D.A. Cheresh, *alphaV integrins in angiogenesis and cancer*. Cold Spring Harb Perspect Med, 2011. **1**(1): p. a006478.
17. Bulte, J.W.M. and M. Modo, *Nanoparticles in Biomedical Imaging: Emerging Technologies and Applications*. 2007: Springer New York.
18. Nagy, J.A., et al., *Heterogeneity of the tumor vasculature*. Semin Thromb Hemost, 2010. **36**(3): p. 321-31.
19. Hood, J.D. and D.A. Cheresh, *Role of integrins in cell invasion and migration*. Nat Rev Cancer, 2002. **2**(2): p. 91-100.
20. van der Flier, A. and A. Sonnenberg, *Function and interactions of integrins*. Cell Tissue Res, 2001. **305**(3): p. 285-98.
21. Haubner, R., S. Maschauer, and O. Prante, *PET radiopharmaceuticals for imaging integrin expression: tracers in clinical studies and recent developments*. Biomed Res Int, 2014. **2014**: p. 871609.

22. Chen, H., et al., *Clinical Application of Radiolabeled RGD Peptides for PET Imaging of Integrin  $\alpha v \beta 3$* . *Theranostics*, 2016. **6**(1): p. 78-92.
23. Beer, A.J., et al., *[<sup>18</sup>F]galacto-RGD positron emission tomography for imaging of  $\alpha v \beta 3$  expression on the neovasculature in patients with squamous cell carcinoma of the head and neck*. *Clin Cancer Res*, 2007. **13**(22 Pt 1): p. 6610-6.
24. Beer, A.J., et al., *Biodistribution and pharmacokinetics of the  $\alpha v \beta 3$ -selective tracer <sup>18</sup>F-galacto-RGD in cancer patients*. *J Nucl Med*, 2005. **46**(8): p. 1333-41.
25. Beer, A.J., et al., *Positron emission tomography using [<sup>18</sup>F]Galacto-RGD identifies the level of integrin  $\alpha(v)\beta 3$  expression in man*. *Clin Cancer Res*, 2006. **12**(13): p. 3942-9.
26. Beer, A.J., et al., *PET-based human dosimetry of <sup>18</sup>F-galacto-RGD, a new radiotracer for imaging  $\alpha v \beta 3$  expression*. *J Nucl Med*, 2006. **47**(5): p. 763-9.
27. Beer, A.J., et al., *Comparison of integrin  $\alpha v \beta 3$  expression and glucose metabolism in primary and metastatic lesions in cancer patients: a PET study using <sup>18</sup>F-galacto-RGD and <sup>18</sup>F-FDG*. *J Nucl Med*, 2008. **49**(1): p. 22-9.
28. Beer, A.J., et al., *Patterns of  $\alpha v \beta 3$  expression in primary and metastatic human breast cancer as shown by <sup>18</sup>F-Galacto-RGD PET*. *J Nucl Med*, 2008. **49**(2): p. 255-9.
29. Beer, A.J., et al., *PET/CT imaging of integrin  $\alpha v \beta 3$  expression in human carotid atherosclerosis*. *JACC Cardiovasc Imaging*, 2014. **7**(2): p. 178-87.
30. Tomasi, G., et al., *Quantification of receptor-ligand binding with [(1)(8)F]fluciclatide in metastatic breast cancer patients*. *Eur J Nucl Med Mol Imaging*, 2011. **38**(12): p. 2186-97.
31. Doss, M., et al., *Biodistribution and radiation dosimetry of the integrin marker <sup>18</sup>F-RGD-K5 determined from whole-body PET/CT in monkeys and humans*. *J Nucl Med*, 2012. **53**(5): p. 787-95.
32. Kim, J.H., et al., *Whole-body distribution and radiation dosimetry of (<sup>68</sup>Ga)-NOTA-RGD, a positron emission tomography agent for angiogenesis imaging*. *Cancer Biother Radiopharm*, 2012. **27**(1): p. 65-71.
33. Iagaru, A., et al., *Glioblastoma Multiforme Recurrence: An Exploratory Study of (<sup>18</sup>F)-FPPRGD2 PET/CT*. *Radiology*, 2015. **277**(2): p. 497-506.
34. Iagaru, A., et al., *(<sup>18</sup>F)-FPPRGD2 PET/CT: pilot phase evaluation of breast cancer patients*. *Radiology*, 2014. **273**(2): p. 549-59.
35. Minamimoto, R., et al., *Biodistribution of the (<sup>18</sup>F)-FPPRGD2 PET radiopharmaceutical in cancer patients: an atlas of SUV measurements*. *Eur J Nucl Med Mol Imaging*, 2015. **42**(12): p. 1850-8.
36. Mittra, E.S., et al., *Pilot pharmacokinetic and dosimetric studies of (<sup>18</sup>F)-FPPRGD2: a PET radiopharmaceutical agent for imaging  $\alpha v \beta 3$  integrin levels*. *Radiology*, 2011. **260**(1): p. 182-91.
37. Withofs, N., et al., *[<sup>18</sup>F]FPPRGD PET/CT imaging of integrin  $\alpha v \beta 3$  levels in patients with locally advanced rectal carcinoma*. *Eur J Nucl Med Mol Imaging*, 2015.
38. Withofs, N., et al., *<sup>18</sup>F-FPPRGD2 PET/CT imaging of integrin  $\alpha v \beta 3$  in renal carcinomas: correlation with histopathology*. *J Nucl Med*, 2015. **56**(3): p. 361-4.
39. Wan, W., et al., *First experience of <sup>18</sup>F-alfatide in lung cancer patients using a new lyophilized kit for rapid radiofluorination*. *J Nucl Med*, 2013. **54**(5): p. 691-8.
40. Mi, B., et al., *Pilot Prospective Evaluation of (<sup>18</sup>F)-Alfatide II for Detection of Skeletal Metastases*. *Theranostics*, 2015. **5**(10): p. 1115-21.
41. Yu, C., et al., *F-Alfatide II PET/CT in healthy human volunteers and patients with brain metastases*. *Eur J Nucl Med Mol Imaging*, 2015.
42. Zheng, K., et al., *<sup>68</sup>Ga-NOTA-PRGD2 PET/CT for Integrin Imaging in Patients with Lung Cancer*. *J Nucl Med*, 2015.
43. Axelsson, R., et al., *An open-label, multicenter, phase 2a study to assess the feasibility of imaging metastases in late-stage cancer patients with the  $\alpha v \beta 3$ -selective angiogenesis imaging agent <sup>99m</sup>Tc-NC100692*. *Acta Radiol*, 2010. **51**(1): p. 40-6.
44. Kenny, L.M., et al., *Phase I trial of the positron-emitting Arg-Gly-Asp (RGD) peptide radioligand <sup>18</sup>F-AH111585 in breast cancer patients*. *J Nucl Med*, 2008. **49**(6): p. 879-86.
45. Chen, H., et al., *Clinical Application of Radiolabeled RGD Peptides for PET Imaging of Integrin  $\alpha v \beta 3$* . *Theranostics*, 2015. **6**(1): p. 78-92.
46. Schnell, O., et al., *Imaging of integrin  $\alpha v \beta 3$  expression in patients with malignant glioma by [<sup>18</sup>F] Galacto-RGD positron emission tomography*. *Neuro Oncol*, 2009. **11**(6): p. 861-70.
47. Zhang, H., et al., *Can an <sup>18</sup>F-ALF-NOTA-PRGD2 PET/CT Scan Predict Treatment Sensitivity to Concurrent Chemoradiotherapy in Patients with Newly Diagnosed Glioblastoma?* *J Nucl Med*, 2016. **57**(4): p. 524-9.
48. Dijkgraaf, I., et al., *Improved targeting of the  $\alpha v \beta 3$  integrin by multimerisation of RGD peptides*. *Eur J Nucl Med Mol Imaging*, 2007. **34**(2): p. 267-73.
49. Dijkgraaf, I., et al., *PET imaging of  $\alpha v \beta 3$  integrin expression in tumours with (<sup>68</sup>Ga)-labelled mono-, di- and tetrameric RGD peptides*. *Eur J Nucl Med Mol Imaging*, 2011. **38**(1): p. 128-37.
50. Terry, S.Y., et al., *Imaging integrin  $\alpha v \beta 3$  on blood vessels with <sup>111</sup>In-RGD2 in head and neck tumor xenografts*. *J Nucl Med*, 2014. **55**(2): p. 281-6.
51. Terry, S.Y., et al., *Can <sup>111</sup>In-RGD2 monitor response to therapy in head and neck tumor xenografts?* *J Nucl Med*, 2014. **55**(11): p. 1849-55.
52. Hong, H., et al., *New radiotracers for imaging of vascular targets in angiogenesis-related diseases*. *Adv Drug Deliv Rev*, 2014. **76**: p. 2-20.
53. Notni, J., et al., *TRAP, a powerful and versatile framework for gallium-68 radiopharmaceuticals*. *Chemistry*, 2011. **17**(52): p. 14718-22.
54. Knetsch, P.A., et al., *[(<sup>68</sup>Ga)]FSC-(RGD)<sub>3</sub> a trimeric RGD peptide for imaging  $\alpha v \beta 3$  integrin expression based on a novel siderophore derived chelating scaffold-synthesis and evaluation*. *Nucl Med Biol*, 2015. **42**(2): p. 115-22.
55. Poethko, T., et al., *Improved tumor uptake, tumor retention and tumor/background ratios of pegylated RGD-multimers*. *Journal of Nuclear Medicine*, 2003. **44**(5): p. 46p-46p.
56. Thumshirn, G., et al., *Multimeric cyclic RGD peptides as potential tools for tumor targeting: solid-phase peptide synthesis and chemoselective oxime ligation*. *Chemistry*, 2003. **9**(12): p. 2717-25.
57. Ma, M.T., et al., *New Tris(hydroxypyridinone) Bifunctional Chelators Containing Isothiocyanate Groups Provide a Versatile Platform for Rapid One Step Labeling and PET Imaging with Ga-68(3+)*. *Bioconjugate Chemistry*, 2016. **27**(2): p. 309-318.
58. Ma, M.T., et al., *Rapid kit-based (<sup>68</sup>Ga)-labelling and PET imaging with THP-Tyr(3)-octreotate: a preliminary comparison with DOTA-Tyr(3)-octreotate*. *EJNMMI Res*, 2015. **5**(1): p. 52.
59. Zhai, C., et al., *Comparison of Ga-68-Labeled Fusarinine C-Based Multivalent RGD Conjugates and [<sup>68</sup>Ga]NODAGA-RGD-In Vivo Imaging Studies in Human Xenograft Tumors*. *Mol Imaging Biol*, 2016.

60. Notni, J., K. Pohle, and H.J. Wester, *Be spoilt for choice with radiolabelled RGD peptides: preclinical evaluation of (6)(8)Ga-TRAP(RGD)(3)*. Nucl Med Biol, 2013. **40**(1): p. 33-41.
61. Ma, M.T.I., C; Cullinane, C.; Roselt, P.; Hicks, R.J.; Blower, P.J., *Enhancing PET signal at target tissue in vivo: A dendritic enneakis(hydroxypyridinone) bifunctional chelator attached to a multimeric alphavbeta3-integrin targeting peptide for molecular imaging with gallium-68*. 2016: Unpublished data.
62. Haubner, R., et al., *Noninvasive visualization of the activated alphavbeta3 integrin in cancer patients by positron emission tomography and [18F]Galacto-RGD*. PLoS Med, 2005. **2**(3): p. e70.
63. Wu, Z., et al., *microPET of tumor integrin alphavbeta3 expression using 18F-labeled PEGylated tetrameric RGD peptide (18F-FPRGD4)*. J Nucl Med, 2007. **48**(9): p. 1536-44.
64. Gladson, C.L., et al., *Stage-specific expression of integrin alphaVbeta3 in neuroblastic tumors*. Am J Pathol, 1996. **148**(5): p. 1423-34.
65. Poethko, T., et al., *Chemoselective pre-conjugate radiohalogenation of unprotected mono- and multimeric peptides via oxime formation*. Radiochimica Acta, 2004. **92**(4-6): p. 317-327.
66. Kubas, H., et al., *Multivalent cyclic RGD ligands: influence of linker lengths on receptor binding*. Nucl Med Biol, 2010. **37**(8): p. 885-91.
67. Rabb, H., et al., *Alpha-V/beta-3 and alpha-V/beta-5 integrin distribution in neoplastic kidney*. Am J Nephrol, 1996. **16**(5): p. 402-8.
68. Lopez-Rodriguez, V., et al., *PET-Based Human Dosimetry of the Dimeric alphavbeta3 Integrin Ligand 68Ga-DOTA-E-[c(RGDfK)]2, a Potential Tracer for Imaging Tumor Angiogenesis*. J Nucl Med, 2016. **57**(3): p. 404-9.
69. McParland, B.J., et al., *The biodistribution and radiation dosimetry of the Arg-Gly-Asp peptide 18F-AH111585 in healthy volunteers*. J Nucl Med, 2008. **49**(10): p. 1664-7.
70. Paulus, W., et al., *Characterization of integrin receptors in normal and neoplastic human brain*. Am J Pathol, 1993. **143**(1): p. 154-63.
71. Chin, F.T., et al., *First experience with clinical-grade ([18F]FPP(RGD(2))): an automated multi-step radiosynthesis for clinical PET studies*. Mol Imaging Biol, 2012. **14**(1): p. 88-95.
72. Davis, P.J., et al., *Membrane receptor for thyroid hormone: physiologic and pharmacologic implications*. Annu Rev Pharmacol Toxicol, 2011. **51**: p. 99-115.
73. Afshar-Oromieh, A., et al., *PET imaging with a [68Ga]gallium-labelled PSMA ligand for the diagnosis of prostate cancer: biodistribution in humans and first evaluation of tumour lesions*. Eur J Nucl Med Mol Imaging, 2013. **40**(4): p. 486-95.
74. Paulino, A.C., et al., *Comparison of CT- and FDG-PET-defined gross tumor volume in intensity-modulated radiotherapy for head-and-neck cancer*. Int J Radiat Oncol Biol Phys, 2005. **61**(5): p. 1385-92.
75. Schinagl, D.A., et al., *Comparison of five segmentation tools for 18F-fluoro-deoxy-glucose-positron emission tomography-based target volume definition in head and neck cancer*. Int J Radiat Oncol Biol Phys, 2007. **69**(4): p. 1282-9.
76. Daisne, J.F., et al., *Tri-dimensional automatic segmentation of PET volumes based on measured source-to-background ratios: influence of reconstruction algorithms*. Radiother Oncol, 2003. **69**(3): p. 247-50.
77. van Dalen, J.A., et al., *A novel iterative method for lesion delineation and volumetric quantification with FDG PET*. Nucl Med Commun, 2007. **28**(6): p. 485-93.
78. Hatt, M., et al., *A fuzzy locally adaptive Bayesian segmentation approach for volume determination in PET*. IEEE Trans Med Imaging, 2009. **28**(6): p. 881-93.
79. Geets, X., et al., *A gradient-based method for segmenting FDG-PET images: methodology and validation*. Eur J Nucl Med Mol Imaging, 2007. **34**(9): p. 1427-38.
80. Disselhorst, J.A., et al., *Optimal Framing in Dynamic FDG-PET*. European Journal of Nuclear Medicine and Molecular Imaging, 2011. **38**: p. S268-S268.
81. Arens, A.I., et al., *FDG-PET/CT in radiation treatment planning of head and neck squamous cell carcinoma*. Q J Nucl Med Mol Imaging, 2011. **55**(5): p. 521-8.
82. Desar, I.M., et al., *Beyond RECIST: molecular and functional imaging techniques for evaluation of response to targeted therapy*. Cancer Treat Rev, 2009. **35**(4): p. 309-21.
83. Hoeben, B.A., et al., *Molecular PET imaging for biology-guided adaptive radiotherapy of head and neck cancer*. Acta Oncol, 2013. **52**(7): p. 1257-71.
84. Hoeben, B.A., et al., *18F-FLT PET during radiotherapy or chemoradiotherapy in head and neck squamous cell carcinoma is an early predictor of outcome*. J Nucl Med, 2013. **54**(4): p. 532-40.
85. Shi, J., et al., *PET imaging of neovascularization with (68)Ga-3PRGD2 for assessing tumor early response to Endostar antiangiogenic therapy*. Mol Pharm, 2014. **11**(11): p. 3915-22.
86. Wen, P.Y., et al., *Updated response assessment criteria for high-grade gliomas: response assessment in neuro-oncology working group*. J Clin Oncol, 2010. **28**(11): p. 1963-72.
87. Rylova, S.N., et al., *Does imaging alphavbeta3 integrin expression with PET detect changes in angiogenesis during bevacizumab therapy?* J Nucl Med, 2014. **55**(11): p. 1878-84.

## Acknowledgements

Last January I started with my final project of the study technical medicine. I have had a great time at the department and have learned many things about conducting research, writing an application that needed to be reviewed by the Medical Ethics Committee, but I also had the opportunity to develop my clinical and laboratory skills. Thanks to **Samantha Terry** I had the opportunity to start this project. Samantha, you have a great passion for conducting research and you have a great professional attitude. Thank you for answering all my questions and sharing your ideas. You give me a lot of inspiration.

I would like to thank my supervisors, **Otto Boerman**, **Wim Oyen**, and **Mark Rijpkema**, for their supervision during this internship, for creating the possibility to work on this research project, and for all those insightful and interesting discussions. Thank you for your supervision, input, suggestions and ideas regarding the (technical) details of the project and this thesis. I am very glad that you give me the opportunity to further develop my knowledge and skills in translational molecular imaging by doing a PhD.

**Cees Slump** and **Bennie Ten Haken**, many thanks for teaching me all the scientific aspects of clinical technology and conducting research. Cees, thank you for being the technical supervisor of this project and Bennie, thank you for being the external member of the exam committee.

I would also like to thank my mentor, **Paul van Katwijk**, for all our conversations and thoughts how I could develop my research skills and how you stimulated me to become a Technical Physician.

Besides my supervisors, I received support from many other colleagues. **Gerben**, **Janneke**, **Desiree**, **Peter**, **Sandra**, **Mijke**, and **Annemarie**, you learned me the basic and more fundamental parts of conducting laboratory science and made me become familiar within the laboratory. Without your help, I would have received many 'snoepjes'. **Willem** and **Charlotte**, thank you for the many discussions and tips concerning the technical parts of the project and thesis.

Furthermore, I would like to thank **Anne Arens** and all other nuclear medicine physicians, for giving me the opportunity to participate in clinical practice and train my medical skills and sharing your ideas about the clinical relevance of many projects.

A special thanks for all other clinicians and laboratory assistants at the department of nuclear medicine, for their guidance and support regarding the clinical study. Another special thanks for all the clinicians, junior doctors in training, and case managers of the department of head and neck oncology. Without their views, critical comments, enthusiasm, and support on the clinical context, we would not have been able to start the clinical study.

Furthermore, I would like to thank all my other colleagues, friends, and family, for their support and motivation and all those moments that have made my study time enjoyable and unforgettable. **Ilse**, thank you for your support in the lay-out of this thesis. **Stijn**, you keep me smiling no matter what.

Last but not least, I would like to thank my parents and my sisters. During all those years I have had your unconditional support to develop myself. Even though it is not always easy, you always support the choices I make. Thank you!

